"Fast Chopper" Time-of-Flight Measurement of Neutron Resonances*

F. G. P. SEIDL, D. J. HUGHES, H. PALEVSKY, J. S. LEVIN, W. Y. KATO,† AND N. G. SJÖSTRAND‡
Brookhaven National Laboratory, Upton, New York

(Received March 23, 1954)

A high-resolution neutron velocity selector, or "fast chopper," has been constructed and is in routine operation at the Brookhaven reactor. It consists of a high-speed rotor that produces bursts of neutrons of about 1-μsec duration, together with a neutron detector at the end of a 20-meter flight path and circuits with which the time of flight is measured. The construction and operating characteristics of the equipment are described briefly. The methods that are used for analysis of sample transmission curves in the energy regions of good and of poor resolution are presented, together with curves used to correct for the effects of Doppler broadening and sample thickness. In the good resolution region the measured total cross section in the vicinity of a resonance can be interpreted to give the total width Γ and $g\Gamma_n$. In the poor resolution region only the quantity $\sigma_0\Gamma^2$, which is proportional to $g\Gamma_n\Gamma$, is obtained. Measured parameters for levels in the 2 to 200 ev energy region are given for silver, iodine, thorium, gold, manganese, and cobalt. The results are compared with theoretical expectations.

I. INTRODUCTION

ALTHOUGH the characteristic features of low-lying levels of some heavy nuclei are reasonably well known from radioactive decay schemes, little detailed information is available on the properties of the levels at excitation energies corresponding to the binding energy of a nucleon. With the use of slow neutrons it is possible in principle to determine the properties of individual nuclear energy levels at an excitation energy just above the neutron binding energy, which is of the order of 7 Mev. For those nuclei in which the first virtual level occurs only one or two electron volts above neutron binding energy, the properties of the level have been determined reasonably well by neutron cross-section measurements. Because of the limited energy resolution available with neutrons, however, it has not been possible until recently to measure the resonance properties for individual levels higher than a few electron volts. Some information has been obtained on the *average* properties of resonances from cross sections at higher energies, which are functions of the level parameters averaged over many resonances. Such studies[1] have shown, for example, that the spacing of levels about one Mev above neutron binding energy exhibits sharp discontinuities at "magic number" nuclei, although it varies smoothly with atomic weight for other nuclei.

In order to exploit the possibility of obtaining detailed information on many levels in individual isotopes by means of neutron resonances, it was important to increase the resolving power of the measuring instruments over that available a few years ago in order to isolate the individual resonances. Study of individual isotopes has assumed greater interest with accumulating evidence that the shell structure of nuclei has a marked effect on the nuclear energy levels. According to the liquid-drop model, used almost exclusively to interpret nuclear structure some years ago, no significant differences would be expected from isotope to isotope other than the minor ones arising from differences in neutron binding energy, which depend in turn on odd-even effects and location relative to the valley of stability. From this point of view there would be no great importance in making detailed measurements on individual isotopes, for any one would be a good representative of others in the same general region of the periodic table.

At the time the present work was begun it seemed certain that, contrary to the liquid-drop model, the ground states and the first few excited states of many nuclei were determined largely by the shell structure of the nucleus. It was not known to what extent the shell structure determined the energy levels at high excitation, however. It seemed likely that at sufficiently high excitation the effect of the shells would disappear and a liquid-drop model would be more appropriate. The capture cross sections[1] at 1 Mev, which gave the average level spacings at energies 1 Mev higher than neutron binding energy, indicated that the shell structure had some effect on the level spacing even after the difference in excitation energy (caused by binding energy discontinuities) was taken into account. The possibility of shell structure extending to high excitation energy was a strong reason for efforts to improve the resolution of neutron spectrometry and for measurements with individual isotopes. During the progress of the work here reported, new developments in nuclear models[2–4] have increased the importance of resonance measurements, because they serve to test the predictions based on these models.

Many of the previous measurements of neutron resonances at low energy had been performed with cyclotron time-of-flight equipment[5,6] or neutron crystal

* Work performed under contract with the U. S. Atomic Energy Commission.

† Now at Argonne National Laboratory, Lemont, Illinois.

‡ Guest physicist from Aktiebolaget Atomenergi, Stockholm, Sweden.

[1] Hughes, Garth, and Levin, Phys. Rev. **91**, 1423 (1953).

[2] Feshbach, Porter, and Weisskopf, Phys. Rev. **90**, 166 (1953).

[3] A. Bohr and B. R. Mottelson, Kgl. Danske Videnskab. Selskab, Mat.-fys. Medd. **27**, No. 16 (1953).

[4] R. G. Thomas (private communication).

[5] Bacher, Baker, and McDaniel, Phys. Rev. **69**, 443 (1946).

[6] Melkonian, Havens, and Rainwater, Phys. Rev. **92**, 702 (1953). This paper gives complete references to earlier papers by this group.

spectrometers[7–14] used with piles. The resolutions available with these two methods were of the same order of magnitude and were sufficient to give the parameters of individual resonances below about 10-ev neutron energy. Recently other time-of-flight instruments of greatly improved resolution have been put into use, namely fast choppers,[15–22] linear electron accelerators,[23–25] and betatrons.[26] The manner in which the improved resolution of these instruments has revealed increased resonance detail is illustrated in Fig. 1, which gives the total cross section of silver as reported in the literature during the last few years.

The most convenient unit for comparing the resolving power of these instruments, whether of the time-of-flight or crystal diffraction variety, is microseconds per meter, that is, the uncertainty in neutron flight time divided by the flight path in meters. The variation of the instrumental resolution with neutron energy is the same for the time-of-flight and the crystal diffraction instruments; hence they all can be compared in units of μsec/m.[27] There is a great difference, however, in the variation of counting rate with energy for the two types of instruments: the intensity per unit time decreases rapidly with energy in the crystal diffraction method but remains almost constant with energy in the time-of-flight instruments. The energy spreads for several values of instrumental resolution are given in Table I as functions of neutron energy. The energy spread is proportional to the resolution (μsec/m) and increases rapidly with neutron energy (as $E^{\frac{3}{2}}$). Most of the cyclotron time-of-flight work was done in the 0.5–1.0 μsec/m resolution range, and the recent instruments have reached approximately 0.1 μsec/m.

In the present paper the Brookhaven chopper will be described briefly; then the methods that have been developed for analyzing resonances will be discussed in detail. Results for several isotopes, as well as the bearing of these results on current nuclear models, will be presented.

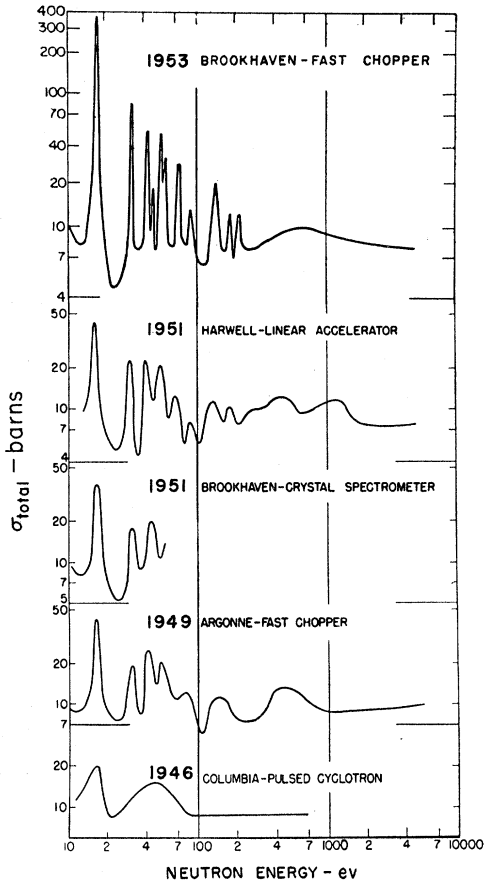

FIG. 1. The total cross section of silver as a function of neutron energy. This figure illustrates the manner in which the improved resolution available in recent years has revealed increased resonance detail in the energy region below 200 ev.

II. APPARATUS

The fast chopper is a mechanical shutter that produces neutron bursts of very short duration by mechanical interruption of a pile neutron beam. The pulses signalling the arrival of the neutrons at a distant detector are sorted into narrow time channels according to the time elapsed after the burst. In this way neutrons of discrete velocities are selected from a beam containing a wide velocity spread, although no true "monochromatic" beam has been produced. The resolution of such time-of-

TABLE I. The energy spreads in ev for several values of instrumental resolution.

Instrumental resolution (μsec/m)	Neutron energy (ev) 1	5	10	50	100	500	1000
0.1	0.0028	0.031	0.088	0.98	2.8	31	88
0.5	0.014	0.155	0.44	4.9	14	155	440
1.0	0.028	0.31	0.88	9.8	28	310	880

[7] W. H. Zinn, Phys. Rev. **71**, 752 (1947).
[8] W. J. Sturm, Phys. Rev. **71**, 757 (1947).
[9] Borst, Ulrich, Osborne, and Hasbrouck, Phys. Rev. **70**, 557 (1946).
[10] L. B. Borst and V. L. Sailor, Rev. Sci. Instr. **24**, 141 (1953).
[11] V. L. Sailor and L. B. Borst, Phys. Rev. **87**, 161 (1952).
[12] V. L. Sailor, Phys. Rev. **91**, 53 (1953).
[13] Foote, Landon, and Sailor, Phys. Rev. **92**, 656 (1953).
[14] R. L. Christensen, Phys. Rev. **92**, 1509 (1953).
[15] W. Selove, Phys. Rev. **84**, 869 (1951).
[16] W. Selove, Rev. Sci. Instr. **23**, 350 (1952).
[17] G. S. Pawlicki and E. C. Smith, Phys. Rev. **87**, 221 (1952).
[18] Seidl, Hughes, and Palevsky, Phys. Rev. **89**, 897 (1953).
[19] Hughes, Seidl, Palevsky, and Levin, Phys. Rev. **90**, 363 (1953).
[20] R. R. Palmer and L. M. Bollinger, Phys. Rev. **91**, 450 (1953).
[21] Bollinger, Thomas, and Palmer, Phys. Rev. **91**, 452 (1953).
[22] Bollinger, Harris, Hibdon, and Muehlhause, Phys. Rev. **92**, 1527 (1953).
[23] A. W. Merrison and E. R. Wiblin, Nature **167**, 346 (1951).
[24] A. W. Merrison and E. R. Wiblin, Proc. Roy. Soc. (London) **A215**, 278 (1952).
[25] Hodgson, Gallagher, and Bowey, Proc. Phys. Soc. (London) **A65**, 992 (1952).
[26] Yeater, Gaerttner, and Baldwin, Phys. Rev. **91**, 451 (1953).
[27] The instrumental resolution of the crystal spectrometer arises from the finite spread in diffraction angle, but this spread corresponds to a fixed uncertainty in μsec/m.

flight equipment depends on (1) the rapidity with which the chopper opens and closes, (2) the distance between the chopper and detector, and (3) the time limits within which the detector and its associated equipment define the arrival of the neutron. The Brookhaven fast chopper has been designed to improve the first factor by its ability to open and close in about 1 μsec. The second factor has been made as favorable as possible by taking advantage of an intensity high enough that a 20-meter flight path can be used. It is possible to reduce the effect of the third factor by making the speed of the electronic equipment faster than the burst time of the chopper. An inherent difficulty arises, however, from the fact that the detector itself may introduce an appreciable uncertainty in the time of arrival of a neutron. Considerable effort is being given to the improvement of the detection apparatus in order to minimize this uncertainty.

A. Chopper

The chopper consists of a stationary slit system (the stator) and a moving slit system (the rotor). From a crudely collimated pile neutron beam the stator produces two sharply defined, slightly divergent beams, and the rotor intercepts these beams except at the moment when the slits of the rotor are aligned with those of the stator. A light beam, which initiates the electronic timing circuits, also passes through the same slit system as the neutrons. The rotor contains eight pairs of slits, the pairs being used to attain as much intensity as possible without sacrificing resolution. However, if more than two slits were employed simultaneously the rotor would not be sufficiently opaque to neutrons.

The shape of the slit system, Fig. 2, is such that each pair of rotor slits opens only once per revolution. The curvature of the trailing edge of the slit is designed to allow the passage of only those neutrons above a certain velocity, the slit closing after the neutrons of minimum velocity have passed through the rotor. Were it not for this elimination of slow neutrons they would reach the detector at the same time as the fast neutrons of the next burst, and this "overlap" would necessitate removal of some of the pairs of slits or a reduction in the flight path.

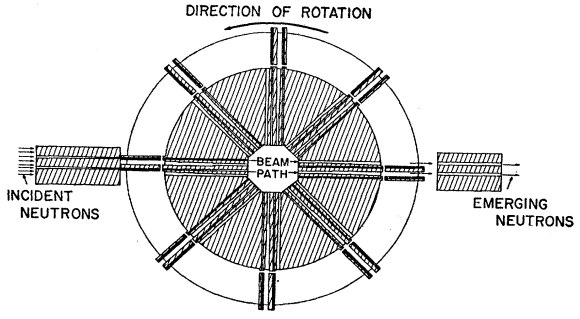

FIG. 2. A schematic plan view of the fast chopper rotor and entrance and exit stators. The shaded areas indicate plastic that is opaque to neutrons. The shape of the slit system is such that each pair of rotor slits opens only once per revolution.

Actually the intensity of even the high-energy neutrons is decreased somewhat by the movement of the rotor during the time these neutrons traverse it. As a result a decrease in intensity, which is minor at high velocities and complete at the cutoff velocity, is produced. The many factors involved in the conflicting requirements of rapidity of the burst, provision of sufficient neutron stopping material for opacity, and large solid angle for intensity, were the subject of extensive analysis of neutron passage through various shutter systems; the present design is the result of these extensive computations.[28]

Because of the many conflicting needs the rotor itself has a somewhat complicated structure, Fig. 3. The assembly containing the slits is made up of a total of 176 pieces of plastic held by two aluminum (14*S*-*T*6) alloy

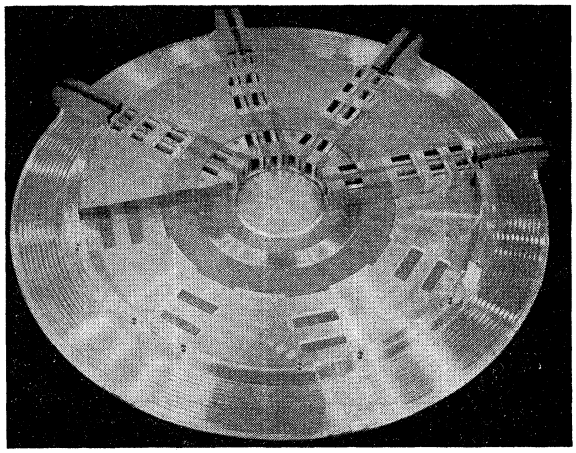

FIG. 3. A photograph of the partly assembled rotor. The 4 pairs of arms enclose the narrowest regions of 4 pairs of rotor slits. The rotor is made up of many pieces of plastic held between two aluminum forgings. It has a 30-in. diameter and weighs 250 pounds.

forgings. It has a 30-in. diameter and weighs 250 pounds. As the present chopper is intended for use in the energy region 10 ev to 10 kev, hydrogen in the form of high-strength phenolic laminate was chosen as the neutron-stopping material because of its high stopping power and low density. With the present design, actual operation showed that for about the first 2° after closing of the slits a slight leakage of high-energy (2-Mev) neutrons occurs by penetration through the phenolic material. These fast neutrons reach the detector in a short time, and at a rotor speed of 6000 rpm, cause some additional background for flight times less than about 40 μsec, corresponding to neutron energies above 1.3 kev. Another obvious difficulty in the use of phenolic laminate as neutron-stopping material is that even between neutron bursts the gamma-ray intensity in the beam is not

[28] The important design factors and the method of construction of the rotor are described in detail by F. G. P. Seidl in a forthcoming Brookhaven National Laboratory report, BNL-278 (*T*-46) (unpublished).

greatly reduced and the neutron detector must therefore have a high discrimination against gamma rays. Some reduction of gamma-ray intensity is obtained by incorporating lead or tungsten in the stator. Tungsten would be useful in stopping the 2-Mev neutrons, but is too heavy for use in the rotor.

The rotor is designed to operate steadily at a speed of 12 000 rpm, at which speed the calculated burst is approximately an isosceles triangle with full width at half-maximum equal to 0.7 μsec. Although the small size of the slit is a result of the attempt to produce a burst of short duration, the intensity being decreased thereby, an advantage results in that exceedingly small samples can be used, in actual practice as small as 20 mg. Lucite sample holders, designed for powdered samples of various thicknesses and of area slightly larger than the slit area (0.0115 in.$\times$1 in.) are used.

A photograph of the rotor and its housing is shown in Fig. 4. The vertical rotation axis represents a distinct difference between the present chopper and those of previous designs, this axis having been chosen because the mechanical problems of operating a high-speed rotor are much simpler for a vertical suspension. The rotor is operated from a dc motor by a $\frac{3}{16}$-in. drive shaft that passes through an oil vacuum seal. The rotor operates at a pressure of about 50 μ of Hg because of the prohibitive drag at atmospheric pressure. The oil vacuum seal is located at the upper part of the drive shaft, which is polished to a high finish. The fact that the present rotor has now operated at 6000 rpm for 18 months with no difficulty illustrates the mechanical simplicity of the vertical suspension. A second rotor has now been built and is being tested for higher speeds; at the present time it has been run at 11 000 rpm for 5 hr. Experimentally some resonance vibration is apparent when the rotor is turning at extremely slow speeds. Above 1000 rpm the rotor spins about its own center of mass with the drive shaft flexing if necessary in order to follow the rotor, and no observable resonance effects are encountered. None of these minor oscillations cause any difficulty in bringing the rotor up to speed, although as a precautionary measure the stator, which is located as close to the rotor as possible at full speed, is removed about $\frac{1}{4}$ in. during the period of acceleration. In case of power failure, or any unusual operation of the electronic circuits, the stator is also moved away automatically.

B. Control and Timing Circuits

Both the electronic circuits to control the chopper and those to time the arrival of neutrons at the detector use a signal from a photomultiplier at the exit collimator of the chopper. By means of mirrors and prisms, light from a tungsten-filament source mounted on the entrance stator is sent down the neutron-beam slits and is reflected onto the photomultiplier, thus ensuring that the neutron burst and light signal are coincident.

The chopper rotor is driven by a dc motor, powered

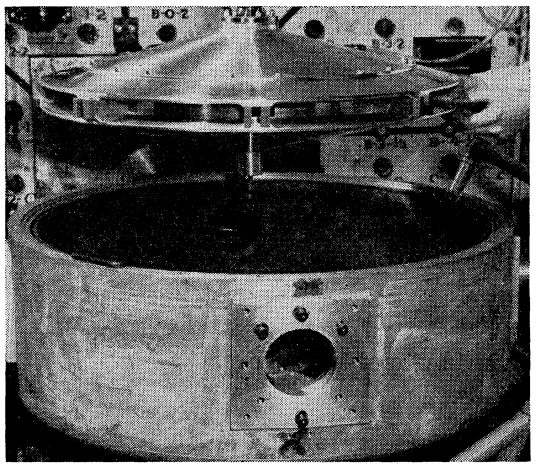

FIG. 4. A photograph of the assembled rotor and its housing. The rotor spins about a vertical axis. Entrance and exit stators are not in place. The pile shield is in the background.

by a motor-generator set. The motor speed is kept constant by an electronic speed controller that accelerates the rotor at 200 rpm per minute to a predetermined speed and maintains that speed to within 0.1 percent. To slow down or stop the rotor the armature circuit may be opened and the rotor will slowly lose speed because of friction and motor windage. To hasten the deceleration the driving motor is used as a generator and the stored energy in the rotor then drives the motor-generator set. The level of this electrical damping is adjustable.

The over-all control system also includes several standard safety features, the main overload protection being a magnetic circuit breaker. Interlocked with the breaker are circuits that open the armature circuit if the vacuum in the chopper housing falls below a predetermined level, if the voltage across the motor rises above a pre-set level, or if any of the voltage supplies for the rotor drive or control system fail. The rotor and its control circuits have now been in operation for about 8000 hr with a minimum of maintenance and repair.

The detector in use at the present time consists of a bank of 2-in. diameter BF_3 proportional counters containing enriched boron. Thirty-five of these counters, connected in parallel, are arranged to fill a volume 10 in. wide, 24 in. high, and 5 in. in the direction of the neutron travel. The efficiency of this bank of counters is extremely low at high energy, for example it is only 0.3 percent at 1-kev neutron energy. The effect of the finite flight path in the detector on the resolution will be discussed later. Although the small sample size is a distinct advantage of the fast chopper in that it allows the use of such rare materials as separated isotopes, the large size of the neutron detector is a disadvantage for it requires many BF_3 counters in the present design or extremely large scintillation counters in other possible designs.

The timing of the neutrons is performed by turning on

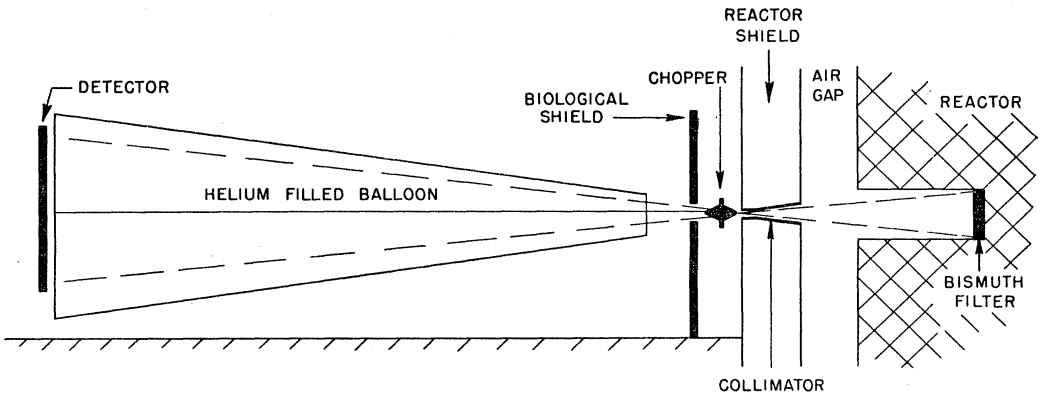

FIG. 5. A schematic elevation view of the arrangement of the chopper at the pile. All dimensions except those of the chopper are approximately to scale. The vertical scale is about 5 times the horizontal scale. The distance between the chopper and the detector is 20 meters.

an oscillator with the light pulse from the photomultiplier, then turning it off with the pulse resulting from the detection of the neutron, a method that results in unusually simple, reliable circuits.[29] The flight time is measured by counting the number of oscillations with a double-decade scaling circuit arranged in a 10×10 matrix. Some time later (but before the next light pulse) a scanning pulse transmits the position where this scaling matrix has come to rest to a bank of 100 registers, one corresponding to each matrix point. The scalers are reset and the system is then ready for another light pulse. The position of the 100 channels may be delayed with respect to the light pulse in steps of 10 channels by means of a coincidence circuit that switches off all pulses from the detector until a pre-set number of oscillations have been counted. The counting of the delay is done by the same 10×10 matrix scaler that generates the channels; in this case it is used as a predetermined count scaler.

Since the transmission and recording of the time of flight can be done in times long compared to the channel width ($\frac{1}{2}$, 1, 2, or 4 μsec channels are available) no fast coincidences are required; the only critical parts of the circuits are the fast scalers which are of standard design. The inability of this system to detect more than one neutron per burst is only a very minor drawback, for the number of detected neutrons of all velocities is very small, only 1/30 per burst at 6000 rpm. The probability of a second count occurring in a particular 100-channel region in the same burst is 1/100 or less, and the resulting loss of counts can be easily calculated.

C. Experimental Arrangement at the Pile

The arrangement at the pile of the chopper, as well as the beam collimator and the detector, is shown schematically in Fig. 5. The particular experimental hole used for the chopper is 4 in. wide by 12 in. high, and extends approximately to the center of the pile. At the far end of the hole, inside the pile lattice, a 12-in. cube of bismuth metal is placed to decrease the intensity of gamma-radiation in the beam. The thermal flux in the pile lattice at the base of the hole is 5×10^{12} neutrons/cm^2 sec. The resonance neutron flux, which is the flux of direct interest for the fast chopper, has a distribution in energy inversely proportional to the energy, i.e., the well-known dE/E spectrum that exists in a graphite moderator. The intensity of the dE/E spectrum relative to the thermal flux is typical of a graphite pile; the number of neutrons in each decade of the dE/E spectrum is given by 1/7 of the thermal flux. The effect of the bismuth block on the neutron intensity was investigated at the time of installation of the chopper and it was found that the presence of the bismuth did not reduce the thermal or resonance flux appreciably, although the gamma-ray intensity was reduced approximately twofold.

In order to lessen the number of neutrons emerging into the open room a series of collimators is located inside the beam hole. These collimators serve to reduce the size of the beam from 4 in.$\times$12 in. high at the base of the hole to two beams, each $\frac{1}{2}$ in.$\times1\frac{1}{2}$ in. high with centers separated by 1 in., at the exit end of the hole. The collimation thus forms two incident beams directed toward the slits of the chopper stator. Even with this beam collimation the neutron intensity is extremely high in the region of the incident stator, and it is necessary to surround the chopper with extensive neutron shielding to keep the neutron intensity in the immediate vicinity below physiological tolerance. The chopper is also surrounded with sandbags and steel plates that serve as an explosion shield; this shield provides additional neutron protection as well.

Samples are inserted in the chopper stator as already described at a point where the beam reaches its smallest size. After leaving the chopper the beam expands in size until it attains an area of about 1 ft$\times$3 ft at the neutron detector 20 meters from the incident end of the rotor. In

[29] The electronic analyzer is described in detail in a forthcoming Brookhaven National Laboratory report by Graham, Higinbotham, and Rankowitz.

this 20-meter flight path the air scattering would be sufficient to reduce the neutron intensity approximately by a factor of two. Practically all this loss is prevented by means of a plastic balloon, filled with helium, extending from the chopper to the detector.

Although some neutron shielding was used around the detector when the chopper was first put in use, at the present time all shielding has been removed from the vicinity of the detector. It was found that even small amounts of shielding near the detector caused some scattering of neutrons back into the detector. These scattered neutrons would have a flight path greater than 20 meters and hence be recorded in an incorrect velocity channel. It was possible to eliminate the shielding at the counters by improving that at the chopper itself, for essentially all the background at the detector arises from neutrons emerging from the fast chopper collimator rather than from general room background.

III. PERFORMANCE CHARACTERISTICS

The equipment is very reliable and operates 24 hr a day, seven days a week, without attention except for sample changing and recording of data. Should a power failure or any change in operating conditions occur that causes the automatic circuits to stop the rotor, part of a run is lost, but as the shutdown is automatic, no attendance is necessary.

The actual counting rate obtained for the open beam is shown in Fig. 6 as a function of flight time; this rate agrees well with an actual calculation based on the resonance flux, the geometry of the chopper, and the efficiency of the detector. The peaks at 1.5 and 2.6 μsec/m are associated with the 12-in. cube of bismuth which is in the pile; the dips at 3.9 and 4.8 μsec/m are due to resonances in the various structural materials that are in the beam. For flight times greater than 3 μsec/m it is seen that the counting rate per channel is nearly constant, exhibiting only a slow decrease with increasing time of flight. This slow decrease represents the so-called chopper function, which is a result of the fact that the slits close partially during the time required by the neutrons to pass through the chopper. Disregarding the chopper function, it is easily seen that the counting rate per channel for a dE/E spectrum and a $1/v$ detector should be constant with time of flight. The flux incident on the counter is dE/E, hence the counting rate will be proportional to $dE/E^{\frac{3}{2}}$, but since the dE represented by a constant channel width dt is proportional to v^3, the counting rate per channel will be constant.

The background, which is also shown in Fig. 6, is about 4 percent of the counting rate at 5-μsec/m flight time and consists about equally of neutrons scattered from the fast chopper hole and alpha disintegrations in the walls of the counters. The background is measured by inserting a 4-in. paraffin block in the beam at the exit stator. Detailed tests, involving intensity measurements as a function of paraffin thickness with the chopper stationary as well as rotating, have shown that the 4-in. paraffin block does not affect the background itself for flight times greater than 2 μsec/m. For most of the cycle (times greater than 2 μsec/m) none of the background originates in the beam itself (such as would be true for background consisting of gamma rays in the beam penetrating the chopper). For times less than 2 μsec/m, however, the background is higher because of the presence of some fast neutrons (about 2 Mev) that penetrate the chopper while it is in a closed position but before the full thickness of plastic has moved into the beam. Background measurements have also been made with thick samples in which the transmission at a resonance was zero for several resolution widths. Although these determinations indicate a slightly higher background rate than that obtained from the paraffin measurements, the difference is not sufficient to affect the accuracy of transmission measurements.

In operation the counting rate is recorded for a given number of counts on a monitor counter rather than as a function of time; the monitor is necessary because of fluctuations in pile intensity. It consists of a single cadmium-shielded BF_3 counter located inside the shielding of the chopper, where it is sensitive primarily to resonance neutrons from the fast chopper hole that are scattered by the stator. Except in special cases where greater accuracy is required, sample runs are made sufficiently long to obtain 2 to 3 percent statistical accuracy per channel in regions between resonances. Comparable accuracy can be obtained much more quickly for the open beam run because for flight times greater than 3 μsec/m the open beam intensity is a slowly varying function, and a smooth curve can be fitted to the data. Background measurements are made periodically during both open beam and sample runs.

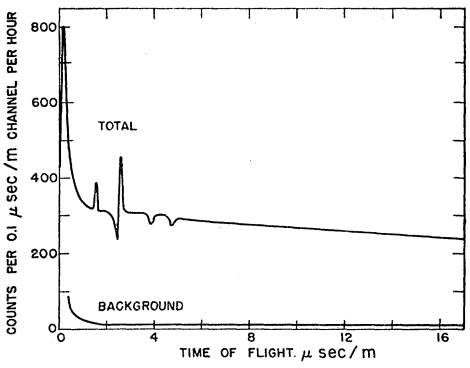

FIG. 6. The open beam and background counting rates as a function of neutron time of flight. The peaks at 1.5 and 2.6 μsec/m are associated with the bismuth filter in the reactor; the dips at 3.9 and 4.8 μsec/m are caused by resonances in structural materials in the beam. The open intensity continues to decrease slowly for flight times greater than 16 μsec/m. The background intensity, which is constant for flight times greater than 2 μsec/m, increases at small flight times because of leakage of fast neutrons.

Although a short burst of neutrons is of fundamental importance in the attainment of high resolution, there are several other points in the apparatus where uncertainties in timing may occur, and it is therefore necessary to ensure that these additional uncertainties in timing are reduced at least to values comparable with the burst time. The additional contributions to the timing uncertainty consist principally of the width of the electronic counting channel, the flight time in the detector, and the delay in the collection of the pulses in the detector. In the present equipment the counting channels are adjustable in steps and the most efficient use of the equipment is attained when the channel time is about equal to the length of the burst. Under present conditions the shortest channel time used is 1 μsec, but $\frac{1}{2}$-μsec channels can be employed when the other timing uncertainties are reduced sufficiently to warrant their use. The time uncertainties involved in the operation of the neutron counters are difficult to decrease and at the present time constitute the major uncertainty in timing, being actually longer than the burst itself.

There exists a variation in collection time in the BF_3 counters which depends on the radial position of the boron disintegration in the counter; the time distribution of this variation for uniform incident flux is a rectangle about 4 μsec wide. This counter "jitter" adds a large amount to the width of the resolution function, an amount that is constant in time for all neutron velocities. The finite length of the counter in the direction of the neutron flight path (13 cm) contributes a constant *fractional* uncertainty of 0.13/20, or 0.6 percent, to the flight time. For high energies this uncertainty in time is small compared to the counter jitter but for low velocities (below 10 ev) the flight time in the counter is the major contribution to the timing uncertainty.

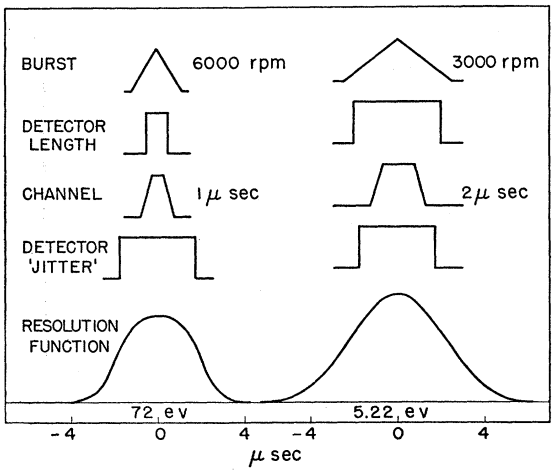

FIG. 7. The calculated resolution function for neutron energies of 72 ev and 5.2 ev. The separate timing uncertainties which contribute to the resolution function are shown. The full width at half-maximum of the resolution function is 0.18 μsec/m (3.0 ev) at 72 ev and 0.25 μsec/m (0.083 ev) at 5.2 ev.

The manner in which the various timing uncertainties combine to give the final resolution function is shown in Fig. 7 for neutron energies of 72 ev and 5.2 ev.[30] An experimental check of this calculated resolution function was made by comparison with a carefully measured transmission function of a sample of silver. The experimental transmission curve for a silver resonance at 72 ev was chosen for the comparison because it should exhibit a shape determined almost completely by the resolution function, for the actual width of the silver resonance is much less than the resolution width at 72 ev. The expected transmission curve for this silver resonance, based on its measured "strength" ($\sigma_0\Gamma^2$ value—to be described later) combined with the 72-ev resolution function of Fig. 7, is compared in Fig. 8 with the measured transmission. It is seen that good agreement exists between the measured transmission curve and that calculated from the resolution function. Thus it appears that the separate contributions to the resolution function are reasonably well known, and that the effective resolution of the instrument for actual transmission measurements is correctly given by the calculation based on these separate components.

Future improvement of the resolution of the entire apparatus obviously depends primarily on improvement in neutron detectors. At the present time development of BF_3 and scintillation detectors for use with the chopper is being actively pursued.[31] A multiple BF_3 counter is being constructed, in which a large number of small diameter proportional counters are mounted in a large container in a common BF_3 atmosphere. The small cathode diameter of these counters as well as the large diameter of the center wire should give a time jitter of 0.5 μsec, which is sufficiently small for the present operating conditions. As this bank of counters is to be 9 cm long in the direction of the neutron travel, the flight time in the counter will still add an appreciable amount to the resolution function for work below 30 ev.

Scintillation counters should be superior to BF_3 counters in both time jitter and size because the time jitter is negligible and a solid scintillator containing enriched boron can be made sufficiently thin that the flight time in the counter will also be negligible. At the present time a combination of fused B_2O_3 and small crystals of ZnS in the form of a large sheet about 1 cm thick seems to be the most promising counter material.[31] The scintillations are detected by a series of photomultipliers connected in parallel and mounted in contact with the sheet. This type of counter is capable of giving high efficiency, of the order of 10 percent for neutrons up to 1 kev, and extremely short time jitter and flight time uncertainties. Until the timing uncertainties of the detector are greatly reduced there is no advantage to be

[30] For the measurements to be described the burst width was actually about 40 percent greater than the calculated value shown in Fig. 7 because of a vertical misalignment of the slits in the stator and rotor. This misalignment has now been corrected. All calculations from Fig. 8 on are based on the wider burst width.

[31] Palevsky, Sjöstrand, and Hughes, Phys. Rev. 91, 451 (1953).

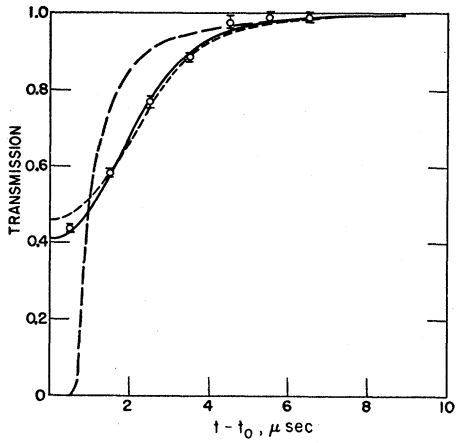

FIG. 8. An experimental check of the calculated resolution function. The — — — curve, calculated from the $\sigma_0\Gamma^2$ value of the 72-ev level in silver, is the transmission curve that would be observed with infinite resolution. The solid and - - - curves were obtained by convoluting the above curve with the resolution function calculated for counter jitters of 3.5 and 4.0 μsec, respectively. The experimental points, obtained with a 6.6 g/cm^2 sample of metallic silver, agree well with the transmission curve calculated for a 3.5-μsec jitter.

gained by operating the chopper above its present routine speed of 6000 rpm.

The 4-μsec jitter in the BF_3 counters causes an average delay of 2 μsec in the arrival of the detector pulse at the analyzer. In order to correct for this and other time delays that might be present in the electronics, a zero correction has been determined by making transmission measurements on the 20-kev group of resonances in titanium.[32] The zero correction is about 3 μsec in magnitude; because of aging of the light source and its associated electronics it can change by about $\frac{1}{2}$ μsec over long periods of time. The correction can easily be redetermined at regular intervals by noting the position of the 2.6-μsec/m peak in the open beam intensity, the energy of this peak having been determined relative to that of the titanium resonances. The energy of this group of resonances has been determined by accelerator measurements to within at least ± 2 kev, which corresponds to $\pm\frac{1}{2}$ μsec for a 20-meter flight path. Since the position of a resonance can be determined with a precision of $\pm\frac{1}{2}$ μsec and the uncertainties in the length of the flight path and the frequency of the analyzer oscillator are each less than 0.1 percent, it is felt that measurements of flight times can be made with an accuracy of ± 1.2 μsec, or ± 0.06 μsec/m.

IV. ANALYSIS OF RESONANCES

Transmission curves obtained with the fast chopper exhibit dips corresponding to resonances in the total cross section of the sample material. Although the separate cross sections, scattering and absorption, that constitute the total cross section are not obviously obtainable from a transmission measurement, we shall see that most of the information needed to determine these cross-section components can in principle be obtained from a measurement of the total cross section. As the relationship between the transmission and the total cross section is extremely complicated, the latter cannot easily be obtained and the analysis is carried out directly on the measured transmission curve. The number of dips observed in a particular energy range gives the level density directly, and further analysis enables the determination of some of the parameters of the resonances.

The cross-section resonances are described by the well-known Breit-Wigner formula, which gives the cross-section variation with energy for energies in which a single resonance level predominates. In the present work it is not necessary to take into account the more complicated formulas that relate to the effect of multiple levels. The one-level Breit-Wigner formula for the cross section as a function of energy, for absorption and for scattering, has the forms[33]

$$\sigma_a=\pi\lambda\!\!\!^{-}_0{}^2 g(E_0/E)^{\frac{1}{2}}\frac{\Gamma_n\Gamma_\gamma}{(E-E_0)^2+(\Gamma/2)^2}, \quad (1)$$

and

$$\sigma_s=4\pi\lambda\!\!\!^{-}_0{}^2 g\left|\frac{\Gamma_n/2}{E-E_0+i\Gamma/2}+\frac{R}{\lambda\!\!\!^{-}_0}\right|^2+4\pi(1-g)R^2, \quad (2)$$

where

$$g=\frac{1}{2}\left[1\pm\frac{1}{2I+1}\right]. \quad (3)$$

In these equations E is the energy of the neutron, $2\pi\lambda\!\!\!^{-}_0$ is the wavelength of a neutron with energy E_0, the energy at resonance, and Γ_n, Γ_γ, and Γ are the neutron, radiation, and total widths of the level. The g factor is a function of the spin I of the target nucleus and is double-valued, corresponding to the two possible spins of the compound nucleus, $I\pm\frac{1}{2}$. The scattering cross section is more complicated than the absorption cross section because of the coherent addition of the resonance and potential scattering amplitudes, the latter arising from scattering by a hard sphere of the nuclear radius, R. The interference effects in the scattering are useful, however, because in certain cases they aid in evaluation of the neutron width of the level.

The total cross section σ_T, which is the sum of the absorption and scattering cross sections, determines the change in transmission observed as a resonance dip, the transmission T being given at each energy by the relationship

$$T=I/I_0=\exp(-n\sigma_T), \quad (4)$$

where I and I_0 are the counting rates observed with and without the sample, containing n atoms per cm^2. If the transmission could be measured with infinite resolution, Eq. (4) would give the cross section as a function of

[32] Hibdon, Langsdorf, and Holland, Phys. Rev. 85, 595 (1952).

[33] J. M. Blatt and V. F. Weisskopf, *Theoretical Nuclear Physics* (John Wiley and Sons, Inc., New York, 1952), pp. 328, 391–4, and 426.

energy directly, from which the level parameters Γ and σ_0 (the peak cross section) could be obtained. Even in this ideal case, however, the separation of the total width Γ into the radiation and neutron widths would require a subsidiary measurement (of the peak scattering cross section or the ratio of scattering to total cross section, for example) because Γ and σ_0 give only $g\Gamma_n$ rather than Γ_n itself. In actual practice, the determination of level parameters is complicated greatly by the finite resolution, which broadens the observed resonance dip, and also by the Doppler effect. Because of the latter, even those neutrons of a single velocity have a velocity spread relative to the target nuclei which are in thermal motion.

The methods of analysis that are used are conveniently divided into those appropriate for two energy regions: a low-energy region of good resolution, where the individual parameters can be determined separately, and a higher-energy region where, as a result of poor resolution, only the combination of parameters $\sigma_0\Gamma^2$ can be determined. In the region of good resolution the actual width and peak height of the resonance can be measured directly from the cross-section curve, if the observed transmission can be corrected for the instrumental resolution. For an energy somewhat higher than that for which the true shape can be obtained, the area of the transmission dip for a thin sample, which gives $\sigma_0\Gamma$, can be combined with $\sigma_0\Gamma^2$ obtained from a thick sample to calculate Γ and σ_0.

In the high-energy region the resolution width is much larger than the natural width of the resonance; hence the shape of the dip in the transmission curve is determined almost completely by the resolution function and the sample thickness. In order to obtain an appreciable dip in the observed transmission curve under such conditions, it is necessary for the sample to be so thick that the true transmission at the peak of the resonance is nearly zero, even though the measured transmission is much higher. The area of the transmission dip in this case gives only the particular combination of parameters $\sigma_0\Gamma^2$, and in the analysis some correction for the Doppler effect must be made. The specific methods that have been developed for use in analysis of the chopper data in these two energy regions will now be described and exemplified by several actual resonances.

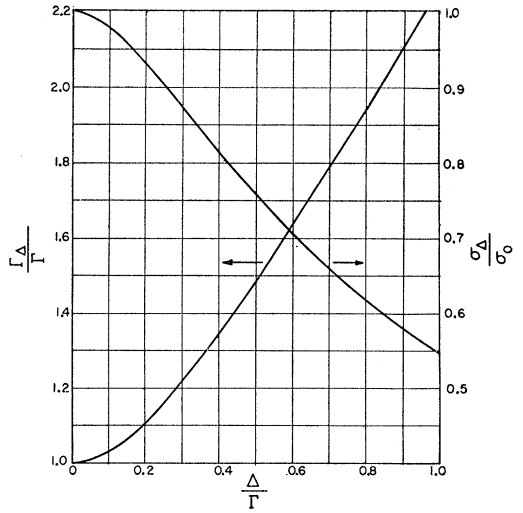

FIG. 9. The ratios Γ_Δ/Γ and σ_Δ/σ_0 as functions of Δ/Γ, where σ_Δ and Γ_Δ are the peak height and full width at half-maximum of a Doppler-broadened resonance, σ_0 and Γ are the peak height and full width at half-maximum of the resonance with no Doppler broadening, and Δ is the Doppler width. For values of Δ/Γ greater than unity, σ_Δ/σ_0 can be evaluated from Eq. (8), and Γ_Δ/Γ can be obtained approximately from the equation $\Gamma_\Delta/\Gamma=0.62+1.66\Delta/\Gamma$.

A. Good Resolution Region

For those cases in which it is possible to obtain the individual parameters of a resonance from transmission curves two general methods of analysis are employed. The first of these makes use of the details of the shape of the observed resonance; the second involves only the areas above transmission dips for several samples of varying thicknesses.

In the first method of analysis the observed transmission curve is corrected for the effects of instrumental resolution, this correction being small in instances where the instrumental resolution is less than the width of the resonance. A formula satisfactory for a small correction can be obtained easily. The true transmission T_{true} is expanded in a power series about the time of flight t for each point; this power series is convoluted with the resolution function $R(t)$ to obtain a series for the observed transmission T_{obs}, and this series is then inverted. For a resolution function that is symmetrical in time, as is the case with the Brookhaven fast chopper, the terms involving odd derivatives drop out and the resulting equation is:

$$T_{\text{true}}(t)=T_{\text{obs}}(t)-\frac{1}{2}T_{\text{obs}}''(t)\int x^2R(x)dx+T_{\text{obs}}^{iv}(t)\times\left[\frac{1}{4}\left(\int x^2R(x)dx\right)^2-\frac{1}{24}\int x^4R(x)dx\right]-\cdots, \quad (5)$$

where $\int R(x)dx=1$. The integrations are to be carried out over the complete extent of the resolution function; hence it is necessary that this function not have long "wings" if the correction is to be small. For those resonances analyzed by the present method the necessary derivatives were obtained with sufficient accuracy by numerical or graphical means, and the correction was sufficiently small that no more terms were needed than are shown in Eq. (5). The true cross section as a function of neutron energy or time of flight follows immediately from the corrected transmission curve by means of Eq. (4).

In general, the cross-section curve obtained in the manner just described will not be that predicted by the Breit-Wigner formula, but will be distorted by the

thermal motion of the target nuclei. The calculation of this Doppler broadening of neutron resonances has been performed by Bethe and Placzek.[34,35] If the $(E_0/E)^{\frac{1}{2}}$ factor (i.e., the $1/v$ factor) and interference effects are neglected in the single level Breit-Wigner formula, and if the target nuclei are assumed to have a velocity distribution characteristic of a free gas, the Doppler-broadened resonance cross section will be

$$\sigma=\frac{\sigma_0}{\Delta\sqrt{\pi}}\int_0^\infty\left[1+\left(\frac{E'-E_0}{\Gamma/2}\right)^2\right]^{-1}\times\exp\left[-\left(\frac{E'-E}{\Delta}\right)^2\right]dE', \quad (6)$$

where the Doppler width Δ is given by

$$\Delta=2(kTE_0m/M)^{\frac{1}{2}}. \quad (7)$$

Here m is the mass of the neutron, M the mass of the target nucleus, T the temperature of the target, and k the Boltzmann constant. Lamb[36] has treated the case of a Debye solid and has shown that if Γ is much greater than $k\theta$, where θ is the Debye temperature, the solid may be treated as a gas at a temperature somewhat greater than its actual temperature. This temperature difference becomes small as the sample temperature becomes much larger than the Debye temperature. Tables and curves of the Doppler-broadened cross section, σ/σ_0, are given by Born,[37] who also gives series for calculating this function and references to other mathematical treatments. In his notation σ/σ_0 is $\psi(x,\eta)$, where $x=(E-E_0)/\frac{1}{2}\Gamma$ and $\eta=\Delta/\frac{1}{2}\Gamma$.

For the method of resonance analysis under consideration, in which the shape of the transmission dip is important, two features of the Doppler-broadened cross section are considered: its peak value σ_Δ and its full width at half maximum, Γ_Δ. The first is easily evaluated analytically from Eq. (8),

$$\sigma_\Delta=\sigma_0\left(\frac{\Gamma}{\Delta}\right)\exp\left[\frac{1}{4}\left(\frac{\Gamma}{\Delta}\right)^2\right]\int_{\frac{1}{2}\Gamma/\Delta}^\infty\exp[-u^2]du. \quad (8)$$

The width is obtained from tables of the function $\psi(x,\eta)$ in the reference by Born[37] and from calculations performed by the authors to extend the range beyond that of the tables. In Fig. 9 are given curves of σ_Δ/σ_0 and Γ_Δ/Γ as functions of Δ/Γ.

In practice, values of Γ_Δ and σ_Δ are obtained from the observed transmission after correction for instrumental resolution in the manner already described. The true parameters, Γ and σ_0, can then be computed by successive approximations using the information from Fig. 9. No attempt is made to obtain σ_0 and Γ by a detailed fit of $\psi(x,\eta)$ to the experimental cross-section curve throughout the entire resonance, as it is felt that the extra labor involved in such an analysis is not warranted by the possible increase in accuracy. Before describing the application of the present "shape" method to a specific resonance, the "area" method will be considered, after which measurement of the 5.2-ev resonance in Ag^{109} by both methods will be described.

The shape method of analysis just discussed requires accurate knowledge of the instrumental resolution function and sufficiently good resolution to observe the details of the resonance shape. In contrast, the method based on the areas above transmission dips is independent of any knowledge of the resolution function and requires only good enough resolution to be able to make statistically significant measurements on a thin sample, one for which $n\sigma_\Delta\lesssim 1$. As a result the area method can be used at somewhat higher energy than the shape method. The accuracy attainable with it, however, is reduced by the fact that only combinations of parameters are obtained.

The area method has been discussed extensively by Melkonian, Havens, and Rainwater.[6] In essence, if the incident neutron intensity changes slowly over the width of the resolution function R, the area "above" a transmission dip (between the transmission curve and unity) is given by

$$A=\int_0^\infty(1-T)dE=\int_0^\infty dE\int_0^\infty[1-e^{-n\sigma(E')}]R(E'-E)dE'. \quad (9)$$

If $\Gamma/2E_0\ll 1$, the lower limits can be replaced by $-\infty$ and the order of integration interchanged, so that

$$A=\int_{-\infty}^\infty[1-e^{-n\sigma(E')}]dE'\int_{-\infty}^\infty R(E'-E)dE, \quad (10)$$

and, since

$$\int_{-\infty}^\infty R(E'-E)dE=1,$$

$$A=\int_{-\infty}^\infty[1-e^{-n\sigma(E)}]dE, \quad (11)$$

which is independent of instrumental resolution.

If the $(E_0/E)^{\frac{1}{2}}$ factor and the Doppler broadening can be neglected in the single-level Breit-Wigner formula, then the integral for the area can be evaluated in terms of Bessel functions of imaginary argument,[38]

$$A=\tfrac{1}{2}\pi n\sigma_0\Gamma\,[\exp(-\tfrac{1}{2}n\sigma_0)][I_0(\tfrac{1}{2}n\sigma_0)+I_1(\tfrac{1}{2}n\sigma_0)]. \quad (12)$$

For a non-negligible Doppler broadening, the integral must be evaluated by series expansion or numerical

[34] H. A. Bethe and G. Placzek, Phys. Rev. **51**, 450 (1937).
[35] H. A. Bethe, Revs. Modern Phys. **9**, 69 (1937), see p. 140.
[36] W. E. Lamb, Jr., Phys. Rev. **55**, 190 (1939).
[37] M. Born, *Optik* (Julius Springer, Berlin, 1933), p. 482.
[38] R. Ladenburg and F. Reiche, Ann. Physik **42**, 181 (1913).

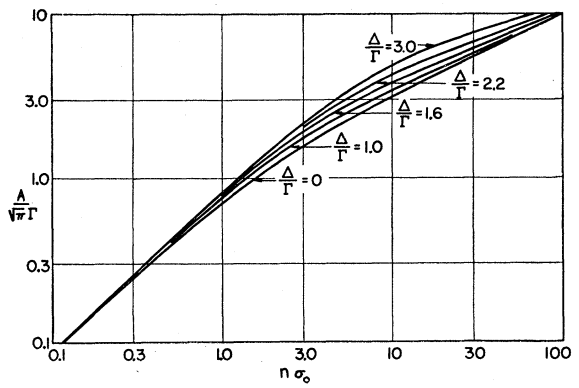

FIG. 10. The ratio $A/\pi^{\frac{1}{2}}\Gamma$ as a function of $n\sigma_0$ for various values of Δ/Γ, where A is the area "above" a transmission dip and n is the sample thickness in atoms/cm². For $n\sigma_0 \ll 1$ the slopes of these curves approach unity; for $n\sigma_0 \gg 1$ the slopes approach $\frac{1}{2}$.

integration. This calculation has been carried out for a wide range of parameters by von Dardel and Persson,[39] and by Melkonian *et al.*[6] These authors assume a single-level Breit-Wigner formula, neglecting the $(E_0/E)^{\frac{1}{2}}$ factor and the interference of resonance with potential scattering. Graphs of $A/\pi^{\frac{1}{2}}\Gamma$ as a function of $n\sigma_0$ for various values of Δ/Γ are shown in Fig. 10. The increase in the area of a transmission dip with increasing temperature (i.e., with increasing Δ) results from the decrease in the effect of "self-protection" that is associated with all but extremely thin samples. Thus the increased temperature makes a sample effectively thinner by reducing the peak height of the resonance; for an extremely thick sample, however, the reduction has little effect.

In the area method, preliminary estimates of σ_0 and Γ are obtained from values in the literature, or from a rough preliminary measurement. These values are then used to select sample thicknesses such that $n\sigma_\Delta \lesssim 1$ for one sample, and $n\sigma_\Delta \gtrsim 10$ for the other, and transmission curves are measured. The analysis to be described is then performed approximately (and none of the corrections discussed are made) in order to obtain rough values of $\sigma_0\Gamma^2$ and $g\Gamma_n/\Gamma$, which are needed in making the corrections necessary in the complete analysis.

The experimental transmission curves for the sample thicknesses described do not reach unit transmission away from the resonance. This fact arises from potential scattering, which is present away from the resonance, or at times simply from instrumental changes in the absolute magnitude of the open beam and sample counting rates. These nonresonance effects are eliminated by multiplying each transmission curve by an appropriate constant to make the transmission approach unity far from the resonance. For a thin sample this constant is easily determined by examination of the wings of the experimental transmission curve. However, for a thick sample this process may be more difficult since, owing to the presence of other resonances, it may not be possible to make measurements sufficiently far away from the resonance for the transmission to be unity.

The resonance shape may also be distorted if there is more than a few percent scattering present in the resonance because of the interference between resonance and potential scattering. In this case, the procedure adopted for normalizing the transmission is to calculate the expected shape of the wings including interference effects, far enough away from the resonance so that effects of Doppler broadening and instrumental resolution can be neglected. In this region the cross section is given by

$$\sigma_T - \sigma_{\rm pot} = \left(\frac{E_0}{E}\right)^{\frac{1}{2}} \frac{\sigma_0\Gamma^2}{4(E-E_0)^2} + \frac{[\sigma_{\rm pot}(\sigma_0\Gamma^2)(g\Gamma_n/\Gamma)]^{\frac{1}{2}}}{E-E_0}, \quad (13)$$

where the first term on the right-hand side arises from the resonance and the other term from the resonance-potential scattering interference. The potential cross section as it appears in the interference term is obtained with sufficient accuracy from published values;[40] the other parameters needed are just those that have already been estimated. The necessary normalizing factor is then obtained by comparing the experimental transmission curve with the calculated curve.

After the transmission curve has thus been normalized to eliminate nonresonance effects, the area above the curve between energies E_0-E_1 and E_0+E_1 is measured.

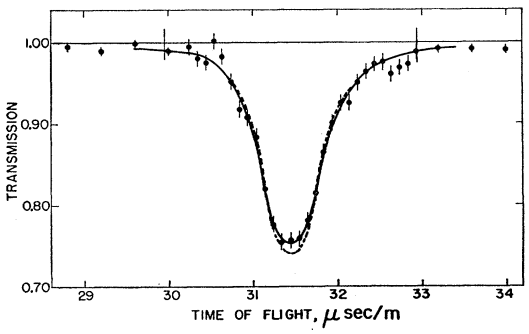

FIG. 11. The normalized transmission as a function of neutron time of flight for the 5.2-ev level in silver, obtained with a thin sample for which $1/n = 72\ 200 \times 10^{-24}$ cm²/atom for Ag^{109}. The solid curve, which is used in the "area" analysis, is drawn through the experimental points; additional data outside of the region shown in the figure verify the fact that the curve approaches unit transmission far from resonance. The vertical lines at approximately 30 and 33 μsec/m indicate the points beyond which the area is calculated rather than measured. The broken curve, which is used in the "shape" analysis, is obtained by correcting the solid curve for instrumental resolution by means of Eq. (5) and the 5.2-ev resolution function of Fig. 7. All errors are given as standard deviations.

[39] G. von Dardel and R. Persson, Nature **170**, 1117 (1952).

[40] *Neutron Cross Sections*, U. S. Atomic Energy Commission Report AECU-2040 (Office of Technical Services, Department of Commerce, Washington, D. C., 1952).

The energy E_1 is selected such that it is much greater than Γ, Δ, and the instrumental resolution, but much less than E_0, and the transmission at E_0-E_1 and E_0+E_1 is greater than 0.9. The area measurement is not continued to higher transmissions because the statistical accuracy of $1-T$ becomes very poor and the effects of other nearby resonances may be important. The neglected area in the wings can be calculated far better from the preliminary $\sigma_0\Gamma^2$ value than it can be measured. Under the conditions set for E_1, the area neglected is given by:

$$\text{Area neglected}=n\sigma_0\Gamma^2/2E_1, \tag{14}$$

with half of this area lying on each side of the resonance. This calculated correction is added to the measured area to give the total area above the transmission curve. A second reason for cutting off the area measurement as discussed above is worthy of mention. The $(E_0/E)^{\frac{1}{2}}$ factor and the interference effects have been neglected in the calculation of the Doppler-corrected area curves (Fig. 10), although both these effects are present in the experimental transmission curve. However, for an area measured in an energy interval symmetrical about E_0, with E_1 small compared to E_0, the contributions to the measured area of the neglected factors cancel to a first approximation if the sample studied is not very thick.

When the area above the transmission curve has been obtained for a given sample, a curve of σ_0 as a function of Γ can then be plotted for that sample. This is done by assuming values of Δ/Γ (and therefore Γ, since Δ can be calculated) and reading $n\sigma_0$ from the appropriate curve of Fig. 10. If the points are plotted on log-log paper with σ_0 as the ordinate and Γ as the abscissa, a slope of minus one is obtained for a thin sample ($\sigma_0\Gamma=$const.), while a slope of minus two corresponds to a thick sample ($\sigma_0\Gamma^2=$const.). For curves obtained from samples of different thicknesses and plotted on the same graph, the point of intersection gives the value of σ_0 and of Γ for the particular resonance. Should these parameters indicate values of $\sigma_0\Gamma^2$ and $g\Gamma_n/\Gamma$ substantially different from those assumed in calculating the corrections to the areas, the analysis can be repeated once more with the new values of the parameters in the corrections. Because of the smallness of the corrections, a single repetition is usually sufficient.

As a test of the "shape" and "area" methods of analysis, a careful study was made of the 5.2-ev level in Ag^{109}. This resonance has been studied most recently by Selove,[15] who used methods and sample thicknesses chosen to avoid the corrections resulting from Doppler broadening. Although the resolution of the Brookhaven chopper is such that the direct shape method can be used on this level to give accurate results, the area method was also applied as a test of the accuracy of the area method.

The transmission curve shown in Fig. 11, which is used for the shape method, was obtained with a silver foil 0.0002 in. thick, for which $1/n=72\,200\times10^{-24}$ cm^2/atom for Ag^{109}. The solid curve is drawn through the experimental points, and the broken curve is obtained by correcting for instrumental resolution, by means of Eq. (5) and the 5.2-ev resolution function from Fig. 7.[30] The correction to the quantity $(1-T)$ is about 5 percent at the minimum of the dip, and is primarily due to the second derivative term; the fourth derivative term is important only in the region where the second derivative is zero. From the corrected curve the transmission at the peak of the resonance is found to be 0.739 ± 0.007. The factors that enter into this error are the statistical accuracy of the experimental curve (±0.005), the statistical accuracy of the normalization of the wings (±0.003), and an estimate of the accuracy of the correction for instrumental resolution (±0.004). (All errors are given as standard deviations.) The experimental peak cross section σ_Δ is $21\,800\pm700$ b, while the full width at half-maximum cross section is 14.4 ± 0.7 μsec, or in energy units, $\Gamma_\Delta=0.239\pm0.011$ ev. Most of the error in the width arises from the uncertainty in the location of the halfway point; the remainder arises from the uncertainty in the shape of the curve in that region.

TABLE II. The parameters of the 5.22-ev resonance in Ag^{109}.

	"Shape" analysis	"Area" analysis	"Best" values	Selove's results[a]
E_0 (ev)	5.22 ± 0.04		5.22 ± 0.04	5.17 ± 0.08
σ_0 (b)	$26\,900\pm1100$	$31\,000\pm3000$	$27\,300\pm1000$	$25\,000\pm3000$
Γ (ev)	0.177 ± 0.014	0.157 ± 0.009	0.168 ± 0.008	0.17 ± 0.02
Γ_n (mv)[b]			12.2 ± 0.5	11 ± 2
$\sigma_0\Gamma$ (ev b)	4750 ± 400	4800 ± 200	4600 ± 200	4300 ± 400
$\sigma_0\Gamma^2$ (ev^2 b)	840 ± 140	755 ± 25	775 ± 25	750 ± 60

[a] See reference 15.
[b] 1 mv $=10^{-3}$ ev.

For silver at room temperature (295°K) Lamb's calculations indicate an effective temperature only 2.6 percent higher than the actual temperature. This effective temperature gives a value of Δ of 0.071 ev at the resonance energy of 5.2 ev. Correction of the observed width for this Doppler broadening gives a true width Γ of 0.177 ± 0.014 ev. The main contribution to the uncertainty in Γ is the error in Γ_Δ; the effect of a 5 percent uncertainty in Δ would be negligible. The ratio Δ/Γ is then 0.40 ± 0.03, σ_Δ/σ_0 is 0.81 ± 0.02, and σ_0 is therefore $26\,900\pm1100$ b. These experimental results, summarized in the first column of Table II, are in good agreement with Selove's results, which are shown in the fourth column of this table.

For the analysis of this resonance by the area method, the transmission curve already given in Fig. 11 is used for the thin sample measurement. It should be noted that for $E_1\ll E_0$ the area above the transmission dip may be evaluated on a plot of transmission against time of flight, since the substitution $dE=(2E_0/t_0)dt$ is then valid. The area can be measured with sufficient accuracy by the use of a planimeter. For the curve of Fig. 11 the area is evaluated between (t_0-19) μsec and (t_0+21) μsec, which represents an energy interval $E_1=0.33$ ev. The area obtained is 0.080 ± 0.003 ev; the error results

from the statistical accuracy of the experimental curve (± 0.002 ev) and of the normalization (± 0.002 ev). The correction for the area in the wings is 0.016 ± 0.001 ev, which is based on the final value for $\sigma_0\Gamma^2$. The error in the wing correction includes an estimate of the uncertainty introduced through neglecting the effects of Doppler broadening and instrumental resolution in the calculation of this correction, as well as a 4 percent uncertainty in $\sigma_0\Gamma^2$. The total area is therefore 0.096 ± 0.003 ev, the wing correction contributing 16 percent.

In Fig. 12 is shown the transmission curve for the thick sample used in the area analysis. This sample is approximately 30 times thicker than the thin sample, having a $1/n = 2110 \times 10^{-24}$ cm^2/atom. In this case the value of E_1 chosen, 1.6 ev, is not small compared to E_0, and it is necessary to evaluate the area on a plot of transmission *vs* neutron energy. The area obtained is 0.949 ± 0.017 ev; 0.012 ev of the error is due to the statistical accuracy of the curve and 0.010 ev to a 0.3 percent uncertainty in the normalization. The correction for the area in the wings is 0.113 ± 0.007 ev, its error arising from the same uncertainties as in the thin-sample case. The total area is therefore 1.06 ± 0.02 ev, the wing correction being 11 percent.

Curves of σ_0 as a function of Γ, with a Δ of 0.071 ev, are given in Fig. 13 for the thick and thin samples just discussed. The broken lines, which represent the uncertainty caused by the errors in the areas, indicate the error in σ_0 for a given value of Γ. The intersection of the two solid lines gives the parameters of the resonance as $\sigma_0 = 30\,800$ b and $\Gamma = 0.157$ ev. Although the order of magnitude of the errors in these quantities can be estimated from the broken lines, a better estimate can be obtained by realizing that the thick and thin sample areas are really measurements of $\sigma_0\Gamma^p$, where p is nearly 2 for the thick sample, and nearly 1 for the thin sample. The values of p, obtained in Fig. 13 from the slopes of the curves at their point of intersection, are 1.91 and 1.06. The quantities which are measured in this example are therefore $\sigma_0\Gamma^{1.91} = 892 \pm 27$ and $\sigma_0\Gamma^{1.06} = 4310 \pm 170$, where σ_0 is in barns and Γ is in ev. From these numbers the uncertainties in σ_0 and Γ are found to be ± 3000 b and ± 0.009 ev, respectively.

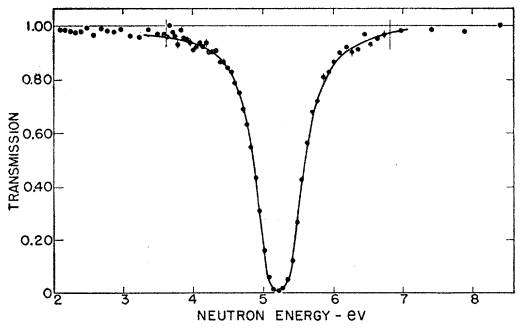

FIG. 12. The normalized transmission as a function of neutron energy for the 5.2-ev level in silver, obtained with a thick sample for which $1/n = 2110 \times 10^{-24}$ cm^2/atom for Ag^{109}. The vertical lines at approximately 3.5 and 7 ev indicate the energies beyond which the area is calculated rather than measured. The curve is normalized by means of Eq. (13) because the effects of the interference term and $(E_0/E)^{\frac{1}{2}}$ factor are appreciable in the wings. The statistical errors are smaller than the points except in the regions where they are indicated.

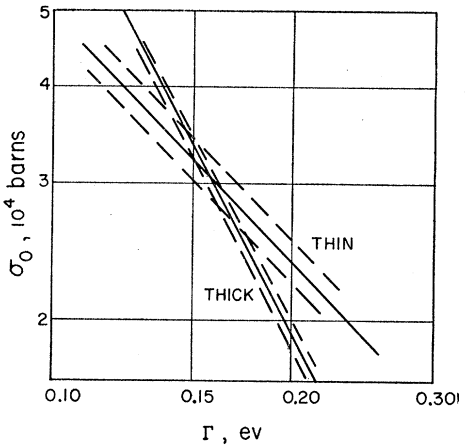

FIG. 13. A plot of σ_0 as a function of Γ for the area analysis of the 5.2-ev level in Ag^{109}. "Thin" and "thick" refer to samples for which $1/n = 72\,200 \times 10^{-24}$ and 2110×10^{-24} cm^2/atom, respectively, for Ag^{109}. The broken lines indicate the error in σ_0 for a given value of Γ. The intersection of the two solid lines gives $\sigma_0 = 30\,800$ b and $\Gamma = 0.157$ ev.

The results of the area measurements are summarized in the second column of Table II. The third column of this table gives "best" values of the parameters of the 5.2-ev level in Ag^{109} obtained by a least-squares fit to the quantities in the first and second columns which were actually measured, that is, σ_0 and Γ for the shape analysis, and $\sigma_0\Gamma^{1.06}$ and $\sigma_0\Gamma^{1.91}$ for the area analysis. From the table it can be seen that the two methods of analysis give results that agree well with each other, and with those of Selove, which are shown in the fourth column. Earlier measurements of the parameters of this resonance, quoted by Selove, agree with Table II but are less accurate. Since Ag^{109} has a spin $I = \frac{1}{2}$, the two choices for the angular momentum of the resonance are $J = 0$ or 1. The expected values of Γ_n/Γ for these possibilities, calculated from the "best" values of σ_0 and E_0, are 0.22 ± 0.01 or 0.073 ± 0.003 for $J = 0$ or 1, respectively. Experimentally, values of Γ_n/Γ are 0.04 as measured by Harris *et al.*,[41] and 0.11 as measured by Sheer *et al.*[42] The correct choice seems to be $J = 1$, which gives a value for Γ_n of 12.2 ± 0.5 mv.

In those cases where corrections for instrumental resolution are small and either the shape or area methods are applicable, the relative accuracy of the two methods is of interest. The area method requires the measurement of a thick sample in addition to the thin sample that is required in both methods, but this fact is not a great disadvantage; the additional time required is

[41] Harris, Muehlhause, and Thomas, Phys. Rev. **79**, 11 (1950).
[42] Sheer, Moore, and Heindl, Phys. Rev. **91**, 449 (1953); U. S. Atomic Energy Commission Report CU-116, 1952 (unpublished).

relatively short since it is much easier to obtain the desired percentage accuracy in area for the thick sample than for the thin sample. As far as the amount of time involved in the analysis is concerned, it is not significantly different for the two methods. With the factors just described taken into account, the following conclusions can be drawn from the analysis of the 5.2-ev Ag resonance:

1. The two methods seem to give equally good values of Γ.
2. If the corrections for instrumental resolution are relatively small, and if $\Delta/\Gamma \lesssim 1$ so that σ_Δ/σ_0 is not very sensitive to errors in Δ/Γ, then the analysis of the resonance shape gives a more accurate value of σ_0.
3. The quantities $g\Gamma_n$ and $\sigma_0\Gamma^2$, which are measures of the area above transmission dips in the limiting cases of thin and thick samples, are best measured by the area method in most cases.

For this example the choice of method of analysis therefore depends on whether the parameters desired are characteristics of the shape of the resonance (σ_0 and Γ), or of the area above the transmission dips ($\sigma_0\Gamma$ and $\sigma_0\Gamma^2$). More generally, the choice would depend upon the energy region, which determines the extent of the distortion of the resonance shape by resolution and Doppler broadening.

B. Poor Resolution Region

At energies where the resolution width is much larger than Γ, the observed transmission curve at a resonance is determined more by the shape of the resolution function and the sample thickness than by the resonance itself. The "shape" method of analysis just described for determination of the level parameters is thus not applicable because of the large corrections that would be necessary to obtain the true shape of the resonance. It also becomes difficult to make the thin-sample transmission measurement necessary for the "area" method because any sample that gives a transmission significantly less than unity (as seen with the actual resolution) is in reality a thick sample. As a result of these experimental conditions, the parameters σ_0 and Γ cannot be determined separately in practice, and only the combination $\sigma_0\Gamma^p$, where p is very nearly 2, is readily obtainable. This quantity results from a thick sample measurement because the cross section in the wings of the resonance, which is proportional to $\sigma_0\Gamma^2$, determines the measured transmission for a thick sample. The actual transmission near the center of the resonance is practically zero; hence its precise value has little effect on the measured transmission.

Corresponding to the decreased information available, there is some simplification in the method of analysis applied to the measured transmission curves, in comparison to the procedure for the good resolution region already described. For example, the wing correction to the area becomes less important, because at high energy the resolution function is much wider than the resonances, whose widths increase only slowly with energy compared to the rapid increase of the resolution width. For predominantly capture resonances the observed transmission rises rapidly to that corresponding to potential scattering, and for the resolution shown in Fig. 7 the wing correction may be neglected for resonances in heavy elements ($A \geq 100$) above about 30 ev.

It is, however, still necessary to make corrections for the effects of Doppler broadening and sample thickness in the calculation of $\sigma_0\Gamma^2$ from the area above the transmission dip for a thick sample. Figure 10, which gives these corrections, can be easily transformed to a form more useful for work with thick samples. The results of this transformation are families of curves giving a correction factor y as a function of the measured area A in ev, for various values of Γ and the Doppler broadening Δ [Eq. (7)]. The correction factor y is defined as

$$y = (\sigma_0\Gamma^2)_{\text{measured}}/\sigma_0\Gamma^2, \tag{15}$$

where

$$(\sigma_0\Gamma^2)_{\text{measured}} = A^2/n\pi. \tag{16}$$

Sets of the correction curves are shown in Figs. 14, 15, and 16 for $\Gamma = 0.05$ ev, 0.10 ev, and 0.20 ev, respectively, which cover the range usually encountered in this parameter. The correction unfortunately depends on Γ, the unknown width of the resonance, but the sample thickness can usually be chosen to make this dependence rather small.

The curves of Figs. 14–16 are convenient for use in measurement of $\sigma_0\Gamma^2$, because they give the magnitude of the Doppler and sample thickness correction much

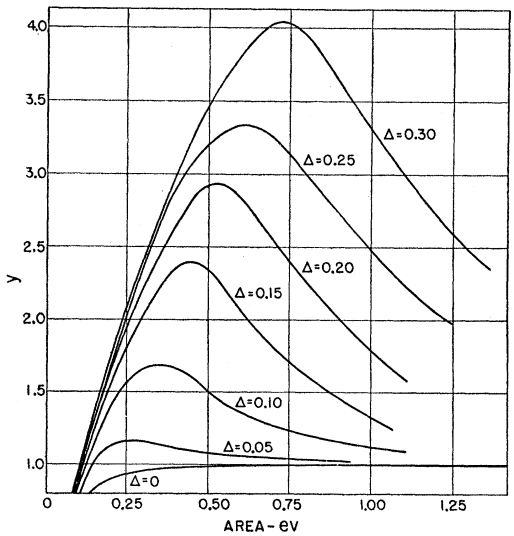

FIG. 14. The correction factor y defined by Eq. (15), as a function of the area above a transmission dip for total width $\Gamma = 0.05$ ev and various values of the Doppler width Δ.

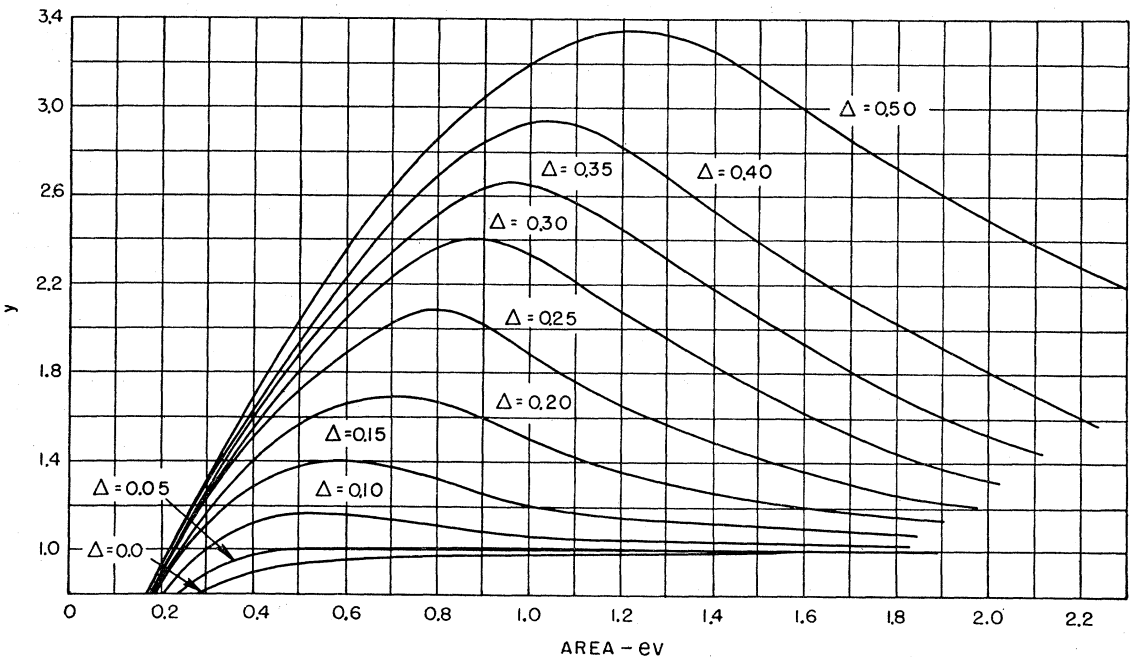

FIG. 15. The correction factor y defined by Eq. (15), as a function of the area above a transmission dip for total width $\Gamma=0.10$ ev, and various values of the Doppler width Δ. For large areas (thick samples) and $\Delta \gtrsim \Gamma$ the correction is small and relatively insensitive to Δ.

This family of curves can be used for values of Γ other than 0.10 ev. For a new set of quantities, Γ', A', and Δ', the value of y is found on the curve for $\Delta=\Delta'/10\Gamma'$ at $A=A'/10\Gamma'$. For example, if $\Gamma'=0.13$ ev, $A'=1.17$ ev, and $\Delta'=0.26$ ev, then $A=1.17/10(0.13)=0.9$, $\Delta=0.26/10(0.13)=0.2$, and from the figure, $y=1.60$.

more directly than do the curves of Fig. 10. In addition they make it possible to estimate readily the error in the correction resulting from uncertainty in the chosen Δ, and thus they aid in choice of a sample thickness to lessen the correction. Plots of y as a function of A for various values of Γ, for a given Δ (an example of which is shown in Fig. 17) can be used to estimate the error in the correction resulting from the uncertainty in Γ. As can be seen from Fig. 17, the correction to the measured $\sigma_0\Gamma^2$ can be obtained with good accuracy for samples of appropriate thicknesses, in spite of the uncertainty in Γ. Fortunately, measurements in the good resolution region indicate that values of Γ_γ do not vary greatly from resonance to resonance in a single isotope nor from isotope to isotope.[43] As a result, the correction y may be made with confidence.

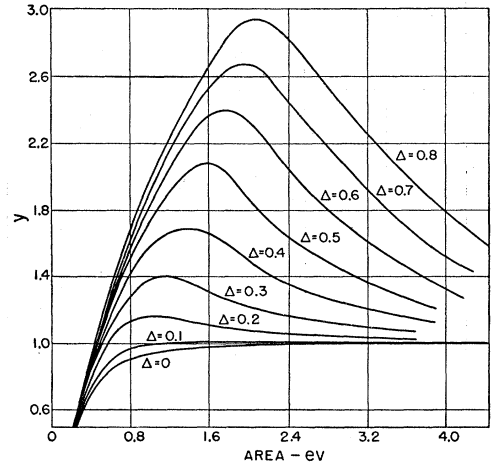

FIG. 16. The correction factor y as a function of the area above a transmission dip for total width $\Gamma=0.20$ ev and various values of the Doppler width Δ.

The procedure for determining $\sigma_0\Gamma^2$ by the area method is one that can be applied to many resonances in a routine manner. The area of a resonance dip, measured as already described, is first used to calculate $\sigma_0\Gamma^2_{\text{measured}}$ from Eq. (16). For the assumed Γ and a Δ, calculated from Eq. (7), the correction factor is obtained from Figs. 14, 15, or 16, by interpolation if necessary. The true value of $\sigma_0\Gamma^2$ is then obtained by dividing $(\sigma_0\Gamma^2)_{\text{measured}}$ by the correction factor y. Should this correction be large, the measurement is usually repeated with a thicker sample in order to make y closer to unity. Figure 17 shows that for a larger area, i.e., a thicker sample for a given resonance, there is a smaller correction, and one that is less sensitive to errors in Γ. It should be noted that with a very thick sample the wing corrections may become appreciable; thus some compromise must be made in sample thickness. The sample should be sufficiently thick for a given resonance to make the correction factor close to unity and insensitive

[43] D. J. Hughes and J. A. Harvey, Nature **173**, 942 (1954).

to changes of Γ, and at the same time not so thick that the wing correction becomes large.

The quantity $\sigma_0\Gamma^2$, obtained by the procedure just described, is not of much interest as such, but it is useful to combine it with an assumed Γ_γ, and hence obtain $g\Gamma_n$. As we shall see later the fluctuations in $g\Gamma_n$ are extremely large compared to the relative constancy of measured values of Γ_γ; hence, assumption of Γ_γ does not involve a serious error. The estimate of the neutron width is made by means of the relation,

$$\sigma_0\Gamma^2=4\pi\lambda\!\!\!^{-}_0{}^2 g(\Gamma_n\Gamma_\gamma+\Gamma_n^2); \tag{17}$$

thus

$$\Gamma_n=\tfrac{1}{2}[(\Gamma_\gamma{}^2+\sigma_0\Gamma^2/\pi\lambda\!\!\!^{-}_0{}^2 g)^{\frac{1}{2}}-\Gamma_\gamma]. \tag{18}$$

For most of the resonances investigated scattering is much less than capture, in which case Eq. (18) reduces to

$$\Gamma_n=\frac{\sigma_0\Gamma^2}{4\pi\lambda\!\!\!^{-}_0{}^2 g\Gamma_\gamma}. \tag{19}$$

The statistical weight g of the resonance is known only in relatively few cases. As can be seen from Eq. (3), if I is zero, $g=1$, and g approaches $\frac{1}{2}$ for large I. For purposes of estimating Γ_n, g is taken to be unity for target nuclei of spin zero, and $\frac{1}{2}$ for all other cases. The maximum error introduced by this assumption is for $I=\frac{1}{2}$, for which the calculated value of Γ_n may be in error by as much as a factor of two. The Γ_n obtained from Eq. (19) seems to depend linearly on the reciprocal of the assumed Γ_γ but the dependence is actually weaker, being linear only for an infinitely thick sample. This result follows from the fact that the assumed Γ_γ is also used in the evaluation of the correction factor y to obtain $\sigma_0\Gamma^2$, and the dependence of Γ_n on Γ_γ is partially canceled. In comparing neutron widths for resonances at different energies, it is useful to eliminate the proportionality of Γ_n to $E_0^{\frac{1}{2}}$ by calculating the reduced neutron width

$$\Gamma_n{}^0=\Gamma_n(\epsilon/E_0)^{\frac{1}{2}}. \tag{20}$$

For convenience, ϵ is taken as 1 ev.

An example of the analysis used in the poor resolution region is furnished by the 31-ev resonance in Ag^{109}. In Fig. 18 the transmission is plotted as a function of time of flight for a 6.6 g/cm^2 sample of silver of normal isotopic composition. The transmission far from the resonance, which is reasonably flat at a value of 0.785 $\pm$0.005, is taken as the transmission representing the potential scattering; this transmission corresponds to a cross section of 6 barns. The area of the dip below the potential scattering is measured as 5.9$\pm$0.5 μsec, which, when normalized to unity transmission to remove the contribution of the potential scattering, becomes 7.6 $\pm$0.7 μsec, or 1.8$\pm$0.2 ev in energy units. The "measured," or uncorrected, $\sigma_0\Gamma^2$ resulting from this area, by Eq. (16), is 60$\pm$12 ev^2 b. The Doppler width Δ is 0.17 ev, calculated as before.

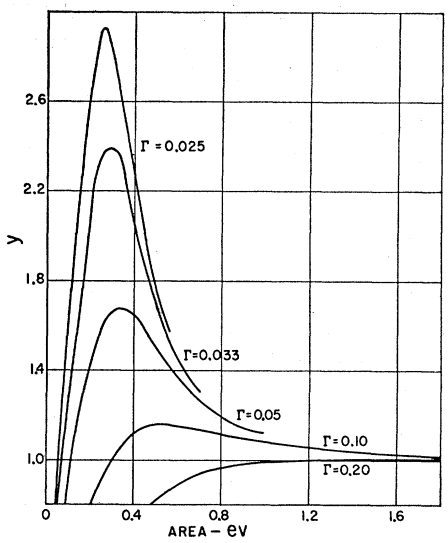

FIG. 17. The correction factor y as a function of the area above a transmission dip for $\Delta=0.10$ ev and various values of Γ. Plots of this type are useful for estimating the error in the correction fatcor that results from an uncertainty in Γ.

In order to calculate the correction factor y, it is necessary to assume a value for Γ. Fortunately the correction factor is not in general very sensitive to the assumed value of Γ if the sample is sufficiently thick. For the present example Γ is taken to be 0.13 ev, a value based on the average of directly measured Γ_γ's in the good resolution region,[43] and on the assumption that $\Gamma\approx\Gamma_\gamma$. From the curves of Figs. 14–16, y is found to be 1.09 and the true $\sigma_0\Gamma^2$ becomes 55$\pm$10 ev^2 b. To indicate the sensitivity of this result to the assumed Γ, calculations are also made for $\Gamma=0.05$ ev and 0.2 ev. These results, summarized in Table III, indicate that in this example y is indeed insensitive to the choice of Γ. On the assumption that $\Gamma=\Gamma_\gamma=0.13$ ev, and the approximation that $g=\frac{1}{2}$ ($I=\frac{1}{2}$ for Ag^{109}), Eqs. (19) and (20) give

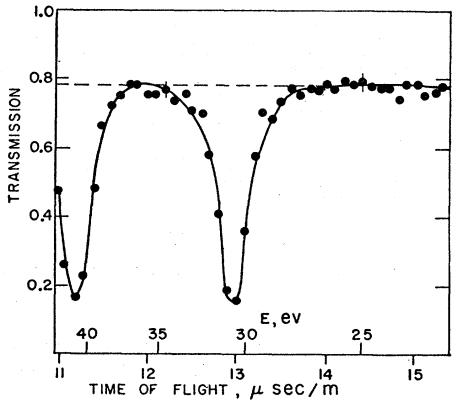

FIG. 18. A plot of transmission as a function of neutron time of flight for a 6.6 g/cm^2 sample of normal silver. The area obtained from this curve is used in the example of Sec. IV B to calculate $\sigma_0\Gamma^2$ for the 31-ev resonance in Ag^{109}. The data are not normalized; the broken line indicates the transmission for potential scattering.

a value of 9 mv for Γ_n and 1.7 mv for Γ_n^0. This result confirms the assumption that scattering is much less than capture for this resonance.

The principal sources of error in the determination of $\sigma_0\Gamma^2$ are the statistical error in the measurement of the area, the error introduced by neglecting the area in the wings, and the error in the area caused by the difficulty in determining the value of the transmission corresponding to potential scattering. The error in the measurement of the area caused by the statistics of the experimental points for the resonance under consideration is about 3 percent. Since the area measurement was stopped about 5 ev away from the resonance, the error in neglecting the area in the wings [Eq. (14)] amounts to about 5 percent of the measured area. The uncertainty in the location of the transmission for potential scattering results in an error in the area of about 4 percent. The combination of these uncertainties produces an error of about 10 percent in the measured area. Since $\sigma_0\Gamma^2$ is proportional to the square of the area, the error in the determination of $\sigma_0\Gamma^2$ caused by uncertainties in the area measurement is about ± 20 percent. As was shown, variation of the assumed Γ by a factor of two changes $\sigma_0\Gamma^2$ by an amount small compared to this 20 percent. Also any uncertainty in the measurement of sample thickness is usually small compared to other errors.

The 31-ev resonance in silver is sufficiently well separated from its neighbors with the present resolution that they do not give rise to any uncertainties in the analysis. At somewhat higher energies, the rapidly increasing spread of the resolution function makes it difficult to locate a transmission between resonances that corresponds to potential scattering, and at still higher energies it is difficult even to distinguish the individual resonances. This increasing difficulty in analysis will be exemplified for silver and other elements in Sec. V.

For many of the resonances analyzed in Sec. V the assumption that $\Gamma_\gamma \gg \Gamma_n$ is not valid. A value of Γ is obtained for these levels by assuming Γ_γ and adding to it a Γ_n obtained from Eq. (18). An iteration process is required to obtain a consistent set of numbers. For several levels it is not feasible to use samples sufficiently thick that the final value of $\sigma_0\Gamma^2$ is insensitive to the assumed Γ_γ. In such cases the estimated error in $\sigma_0\Gamma^2$ includes an uncertainty in y produced by a 20 percent uncertainty in the assumed Γ_γ.

V. RESULTS

An extensive program of energy level study is now under way which makes use of the methods of analysis described in the previous section. In this work the identification of energy levels with individual isotopes usually necessitates the use of separated isotopes, and in this respect the small sample size of the fast chopper is a great advantage. Total cross sections alone have been measured; the only uncertainty in the determination of parameters that results from this procedure is the uncertainty in g; and at the present stage of neutron spectroscopy this is not significant. The main advantage of additional measurements of scattering or absorption, which would give g, would be in the resulting knowledge of the level spin J.

The general program consists of measurement of individual level parameters at low energy, where good resolution makes such determinations possible, together with measurement of $\sigma_0\Gamma^2$ alone for resonances in the poor resolution region. This latter quantity is used to obtain values of Γ_n, on the assumption that the variation of Γ_γ from resonance to resonance is so much less than that of Γ_n that values of Γ_γ obtained from low energy resonances may be used in the analysis. The results of the measurements to date show that this assumption is justified and that the values of Γ_n thus obtained are reasonably accurate. When higher resolution is available with the fast chopper, individual parameters can be measured for additional resonances and the validity of the assumption concerning Γ_γ investigated in more detail. The results for several elements will be considered at present and the findings concerning level densities and widths discussed briefly. Additional measurements with the fast chopper, not included in this report, have been presented recently.[44–48]

TABLE III. The dependence of the final value of $\sigma_0\Gamma^2$ for the 31-ev resonance in Ag^{109} on the assumed Γ used in the calculation.

Γ	0.05 ev	0.13 ev	0.20 ev
y	1.13	1.09	1.05
$\sigma_0\Gamma^2$	53 ev² b	55 ev² b	57 ev² b

A. Manganese and Cobalt

When the fast chopper was first put into operation, some measurements were made on medium weight nuclei with well-separated resonances to test its performance. Manganese and cobalt were suitable for this purpose since their level spacings were sufficiently great that the first few resonances should not overlap and furthermore both had been investigated with other velocity selectors. The fact that the resonances in both these elements are almost completely scattering[41] also simplified the analysis greatly.

A previously unknown resonance, shown in the cross-section curve of Fig. 19, was found in Mn^{55} at 1120 ± 60 ev. This level had not been observed before because of the very poor resolution available in this energy region which lies between those that were covered by the time-of-flight[49] and Van de Graaff[32] measurements, also

[44] Hughes, Kato, and Levin, Phys. Rev. **92**, 1094 (1953).
[45] Kato, Hughes, and Levin, Phys. Rev. **93**, 931 (1954).
[46] J. S. Levin and D. J. Hughes, Bull. Am. Phys. Soc. **29**, No. 4, 57 (1954).
[47] R. S. Carter and J. A. Harvey, Bull. Am. Phys. Soc. **29**, No. 4, 57 (1954).
[48] Pilcher, Carter, and Stolovy, Bull. Am. Phys. Soc. **29**, No. 4, 57 (1954).
[49] Rainwater, Havens, Wu, and Dunning, Phys. Rev. **71**, 65 (1947).

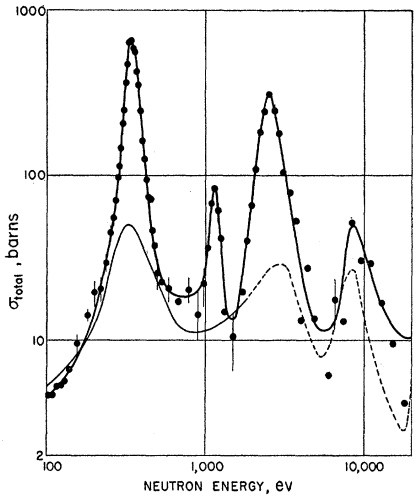

FIG. 19. The total cross section of Mn^{55} as a function of neutron energy. A 0.46 g/cm² sample of manganese was used to make the measurements above 150 ev. A previously unknown resonance was found at 1120 ev; this level lies between the energy region well covered by the earlier time-of-flight measurements (see reference 49) (light solid line) and that well covered by Van de Graaff measurements (see reference 32) (broken line). The fast chopper measurements bridge this gap, and below 4 kev provide better resolution than is available with present-day Van de Graaff measurements. The peak heights shown in this figure are not the true peak heights of the resonances, but are distorted by the instrumental resolution; higher values would be observed with a thinner sample.

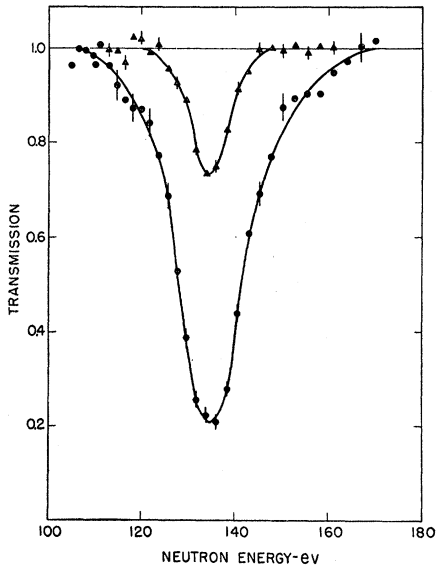

FIG. 20. The normalized transmission as a function of neutron energy for thin ($1/n=22\,200\times10^{-24}$ cm²/atom) and thick ($1/n=2230\times10^{-24}$ cm²/atom) samples of Co^{59}. These measurements were used in the area analysis of Sec. V A to obtain parameters of the 134-ev resonance.

shown in Fig. 19. This example illustrates the value of the fast chopper in bridging the gap that formerly existed between these two types of measurements. The presence of this resonance has since been confirmed by measurements with other time-of-flight instruments.[50,51]

Parameters were determined for the level at 346±11 ev by fitting the shape of the cross-section curve between 150 ev and 250 ev with a single-level Breit-Wigner formula that included interference between resonance and potential scattering; the thickness of the Mn metal sample was 2.4 g/cm². In this energy region the cross section is dominated by the 346-ev level and the effects of instrumental resolution are negligible. The analysis yielded $\sigma_0\Gamma^2=(3.0\pm0.6)\times10^6$ ev² b, and since the resonance is almost completely scattering, it follows that $g\Gamma_n=20\pm2$ ev. The spin of Mn^{55} is 5/2; therefore $\Gamma_n=31\pm3$ ev or 26±3 ev for $J=2$ or 3, in agreement with the work of Harris *et al.*[52] They selected $J=3$ as the correct value of the spin of the compound state. If most of the 13-barn thermal cross section is associated with the 346-ev level, then this measurement gives a value of 0.5±0.1 ev for the radiation width of the resonance.

Measurements were made on the 134±2 ev resonance in Co^{59} in order to determine σ_0 and Γ by the "area" method and to see if J could thus be determined for this level. Although Doppler broadening is negligible ($\Delta/\Gamma\approx0.1$), a resolution of 0.18 μsec/m was not adequate for use of the "shape" method of analysis because this resolution width was almost twice the width of the resonance. Normalized transmission curves are shown in Fig. 20. The areas above the transmission dips, including a correction for the area in the wings, were 3.22±0.16 ev and 17.9±0.5 ev for samples with $1/n=22\,200\times10^{-24}$ and 2230×10^{-24} cm²/atom, respectively. The samples used were solutions of $CoSO_4$ in heavy water. Neither sample was so thick that the interference between resonance and potential scattering would introduce any appreciable error in the analysis. Parameters for this level, obtained from these areas, are $\sigma_0=9700\pm1800$ b, $\Gamma=5.2\pm0.7$ ev, $\sigma_0\Gamma=51\,000\pm3000$ ev b, and $\sigma_0\Gamma^2=260\,000\pm16\,000$ ev² b. The value of $\sigma_0\Gamma^2$ agrees with previously published values.[24] Reference 24 also includes references to earlier measurements on cobalt.

As the spin of Co^{59} is known to be 7/2 and as the level is primarily scattering (Γ_n/Γ about 0.95),[41] the two possible values of σ_0 are 8200 b for $J=3$, or 10 600 b for $J=4$. Unfortunately the value of σ_0 here obtained is not sufficiently accurate to chose between these two values and permit an assignment of J for the level. Earlier measurements on this resonance had been made by Seidl.[53] This experiment consisted of measuring the transmission of a thin cobalt foil as a function of the thickness of a boron absorber placed in the neutron beam, by using a detector that was selectively sensitive to neutrons scattered by the cobalt resonance. The results of the experiment were consistent with either $\Gamma=2.0\pm0.1$ ev and $J=4$ or $\Gamma=5.0\pm0.5$ ev and $J=3$.

[50] L. M. Bollinger (private communication).
[51] Albert, Yeater, and Gaerttner (private communication).
[52] Harris, Hibdon, and Muehlhause, Phys. Rev. **80**, 1014 (1950).
[53] F. G. P. Seidl, Phys. Rev. **75**, 1508 (1949).

These values, when considered with the present measurements, indicate that $J=3$ is the best choice for the spin of the compound state of this resonance.

B. Silver

Practically all the fast chopper work has been devoted to the resonances in the first few hundred volts for isotopes of atomic weight greater than 100. Under these conditions the high resolving power of the fast chopper is of great value in analyzing the close resonances that occur and the results have a direct application to the theories of the structure of heavy nuclei.

Transmission measurements of samples of normal silver metal, 99.9 percent pure, were made in the energy region from 5 to 200 ev. Some of these measurements and their analysis have already been presented as examples in Secs. IV A and IV B. The total cross section as a function of energy, calculated from these measurements by means of Eq. (4) with no correction made for instrumental resolution and Doppler broadening, is shown in Fig. 21. The cross-section curve thus obtained is of course only a qualitative description of the true cross section, for as has been seen the resonances are distorted by instrumental resolution and Doppler broadening. Measurements on silver by other experimenters are given in references 15 and 24.

Transmission measurements were also made with electromagnetically enriched samples of silver isotopes, obtained from the Isotopes Division at Oak Ridge National Laboratory. Transmission curves for these separated isotopes, as well as for normal silver, are shown in Fig. 22. The high isotopic purity of these samples (>96 percent of the isotope of interest) made it a simple procedure to assign all the resonances below 100 ev. The resonance observed in normal silver at about 41.5 ev was found to be two levels, one in Ag^{109} at 40.8 ev, and the other in Ag^{107} at 42.4 ev. The two resonances between 50 and 60 ev were also completely separated. The isotopic assignments are shown in the second column of Table IV. The resonances above 100 ev are probably not resolved with the present instrumental resolution and no isotopic assignments are made.

Values of $\sigma_0\Gamma^2$, calculated as in the discussion of Sec. IV B, are shown in column 7 of Table IV. In the corrections for Doppler broadening and sample thickness, Γ_γ was assumed to be 0.13 ev, an average value of experimentally determined radiation widths in the region of atomic weight 110.[43] Areas were obtained from the measured transmission curves for normal silver except in those cases where the levels were adequately resolved only by the use of separated isotopes. The areas that were measured with separated isotope samples were not used for all the levels because in general these samples were not thick and the corrections were therefore rather large. The last two columns of Table IV give values of $2g\Gamma_n$ and $2g\Gamma_n^0$, calculated from Eqs. (19) and (20) by assuming $\Gamma_\gamma=0.13$ ev. Since g is unknown for all but the 5.2-ev level ($I=\frac{1}{2}$ for both isotopes of silver), these columns correspond to Γ_n and Γ_n^0 under the approximation that $g=\frac{1}{2}$. In the calculation of the *average* reduced neutron width, $\bar{\Gamma}_n^0$, little error is introduced by this approximation. Except for the one small resonance at 45.6 ev the values of Γ_n^0 are reasonably constant.

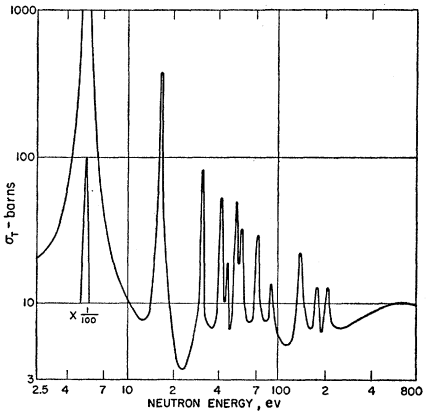

FIG. 21. The total cross section of Ag as a function of neutron energy. The 42-ev "level" is composed of two resonances, one in each isotope. Above 100 ev individual levels were not resolved. Observed cross sections near resonance are not the true values, but are lowered by the effects of instrumental resolution and Doppler broadening.

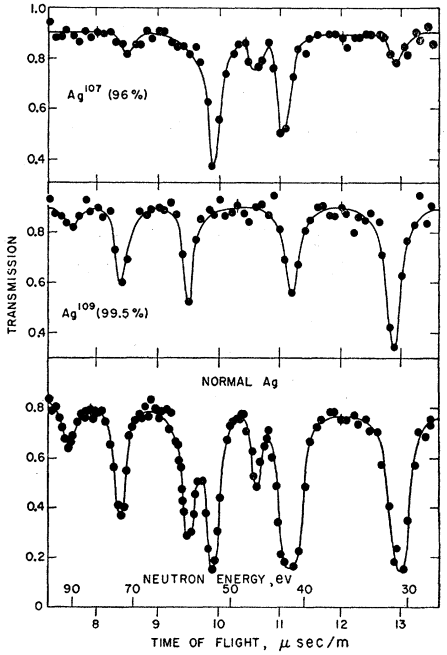

FIG. 22. The transmission as a function of neutron time of flight for samples of isotopically enriched silver and of normal silver. The Ag^{107} sample contained 1.20 g/cm² of Ag^{107}, the Ag^{109} sample 0.82 g/cm² of Ag^{109}, and the sample of normal silver 3.4 g/cm² of Ag^{107} and 3.2 g/cm² of Ag^{109}. The calculated contribution of the 4 percent Ag^{109} to the transmission of the Ag^{107} sample agreed with the dips observed at 31, 57, and 72 ev. The 42-ev "level" appeared to be too wide in the normal Ag sample, but in the enriched samples it was resolved into two levels (one in each isotope) at somewhat different energies.

TABLE IV. A summary of the parameters of the levels from 0 to 100 ev in Ag^{107} and Ag^{109}. Γ_γ is assumed to be 0.13 ev.

E_0 ev	Isotope	Area ev	$(1/n)\times10^{24}$ cm²/atom	Δ ev	y	$\sigma_0\Gamma^2$ ev² b	$2g\Gamma_n$ mv	$2g\Gamma_n^0$ mv
5.22±0.04[a]	109			0.071		775±25	12.2± 0.5	5.3 ±0.2
16.6 ±0.15	107	1.9 ±0.2	52.4	0.13	1.03	60± 7[b]	5.6± 0.8	1.4 ±0.2
31.1 ±0.4	109	1.8 ±0.2	56.3	0.17	1.09	52± 6[b]	9 ± 2	1.6 ±0.3
40.8 ±0.6	109	0.82±0.12[c]	220	0.20	1.41	34±10	8 ± 3	1.2 ±0.4
42.4 ±0.6	107	1.1 ±0.2[c]	150	0.20	1.31	45±15	10 ± 4	1.6 ±0.6
45.6 ±0.7	107	0.85±0.08	52.4	0.21	1.50	8± 2	2.1± 0.6	0.31±0.09
52.2 ±0.8	107	2.9 ±0.6	52.4	0.22	1.04	140±40		
		2.0 ±0.2[c]	150		1.13	165+40		
					Average	150±30	36 ±10	5.0 ±1.4
56.8 ±0.9	109	2.5 ±0.5	56.3	0.23	1.09	100±40		
		1.3 ±0.2[c]	220		1.31	90±30		
					Average	95±25	24 ± 6	3.2 ±0.8
72.5 ±1.3	109	3.0 ±0.3	56.3	0.27	1.10	150±30	47 ±15	5.5 ±1.8
88.5 ±2	109	1.34±0.14	56.3	0.29	1.55	21± 5	10 ± 3	1.1 ±0.3

	Ag^{107}	Ag^{109}
$\bar{\Gamma}_n^0$	2.1 mv	3.0 mv
D	50 ev	33 ev

[a] The results for this resonance are taken from the third column of Table II, with $g=\frac{3}{4}$. The numbers in the last two columns are Γ_n and Γ_n^0.
[b] Average of four measurements with samples of different thicknesses.
[c] Measured with isotopically enriched samples.

These values can be expected to vary by a factor of three just because of the fact that the J value of the levels are not known. Above 100 ev the reduced neutron widths become much larger; this fact is taken to indicate that the observed "levels" are multiple, the actual levels not being resolved.

On the assumption that all the resonances below 100 ev have been resolved, the average spacing of levels D was calculated. This spacing refers to levels of a single J that are a result of $l=0$ interactions and that lie at an excitation energy just above the neutron binding energy. The level spacing was estimated by dividing the energy interval considered by the number of levels found in that interval, and doubling this number on the assumption that half of the levels are in each spin state. The level spacing is 50 ev and 33 ev in Ag^{107} and Ag^{109}, respectively. Arithmetic averages of the reduced neutron widths $\bar{\Gamma}_n^0$, for these isotopes are 2.1 mv and 3.0 mv, respectively. It is almost certain that for the energy region below 100 ev all levels for $l=0$ interactions in these isotopes have been found. At 100 ev any resonance with a Γ_n^0 larger than 1/20 of $\bar{\Gamma}_n^0$ would have been seen; at lower energies even weaker resonances would have been detected.

C. Iodine

Transmission measurements of samples of elemental iodine, 99.9 percent pure, were made in the energy region from 15 to 200 ev; it is known from the work of other experimenters[24] that there are no neutron resonances below 15 ev. A cross-section curve is shown in Fig. 23. The resonance structure is much more clearly resolved here than in earlier measurements by others. The parameters of the resonances up to 100 ev, measured in the manner described for silver, are summarized in Table V. Above 100 ev the levels were not well resolved and therefore were not analyzed, whereas below 100 ev it seems certain that all $l=0$ resonances are represented. The calculated parameters are based on a value of Γ_γ of 0.10 ev.

On the assumption that all the resonances below 100 ev have been resolved, the average level spacing for states of a given J in iodine is 29 ev. The average value of Γ_n^0 for these levels is 2.8 mv. The observed values of $2g\Gamma_n^0$ show fluctuations of a factor of 20; as the spin of I^{127} is 5/2, lack of knowledge of J can produce variations of only a factor of 1.4. It can be concluded that the fluctuations in Γ_n^0 are much larger than those which have been observed in Γ_γ;[43] thus, any minor fluctuations in Γ_γ will not appreciably affect the calculation of Γ_n^0.

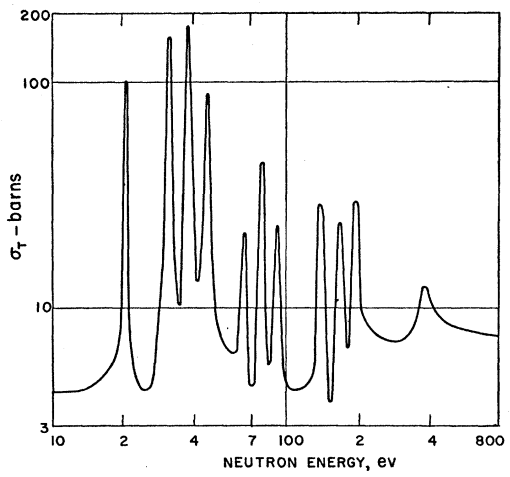

FIG. 23. The total cross section of I^{127} as a function of neutron energy. There are no resonances below 20 ev; above 100 ev individual levels were not resolved. Observed cross sections near resonance are not the true values, but are distorted by the effects of instrumental resolution and Doppler broadening.

TABLE V. A summary of the parameters of the levels from 0 to 100 ev in iodine. Γ_γ is assumed to be 0.10 ev.

E_0 ev	Area ev	$(1/n)\times10^{24}$ cm²/atom	Δ ev	y	$\sigma_0\Gamma^2$ ev² b	$2g\Gamma_n$ mv	$2g\Gamma_n^0$ mv
20.5±0.3	0.70±0.07	80.0	0.13	1.24	10± 3	1.6± 0.5	0.35±0.11
31.4±0.5	2.1 ±0.2	80.0	0.16	1.03	105±30	21 ± 7	3.8 ±1.3
37.7±0.7	2.7 ±0.3	80.0	0.17	1.04	180±50	38 ±13	6.0 ±2.0
46 ±1	1.8 ±0.3	80.0	0.19	1.13	75±30	21 ± 9	3.2 ±1.4
66 ±2	1.0 ±0.4	25.2	0.23	1.70	5^{+9}_{-3}	$2.3^{+4}_{-1.5}$	$0.3^{+0.5}_{-0.2}$
78 ±2	1.7 ±0.4	80.0	0.25	1.26	60^{+50}_{-30}	30^{+25}_{-15}	$3^{+3}_{-1.5}$
91 ±3	2.6 ±0.8	25.2	0.27	1.07	50^{+50}_{-25}	30^{+30}_{-15}	$3^{+3}_{-1.5}$
			$D=29$ ev		$\bar{\Gamma}_n^0=2.8$ mv		

D. Gold

Transmission measurements of samples of high-purity gold metal were made in the energy region from 3 to 300 ev. A transmission curve for a sample thickness of 12.3 g/cm² is shown in Fig. 24 for energies above 30 ev. Below 30 ev there is only one resonance, at 4.9 ev. The asymmetry of the 61.5-ev level and the slope of the transmission curve between 30 and 50 ev are caused by interference between resonance scattering and potential scattering. This interference term falls off slowly, only as the first power of the reciprocal of $E-E_0$. The asymmetry occurs because the interference term changes sign at resonance.

The parameters of the 4.94-ev level were obtained by analysis of the shape of the transmission dip for a 0.00465 g/cm² sample, by using the method described in Sec. IV A. The maximum observed cross section was 25 000±800 b and the observed width at half the maximum cross section was 0.23±0.01 ev. Correcting for instrumental resolution gave $\sigma_\Delta=26\,500\pm1000$ b, and $\Gamma_\Delta=0.20\pm0.01$ ev. For a Doppler width of 0.051 ev the parameters of this level are $\sigma_0=30\,600\pm1500$ b, and $\Gamma=0.163\pm0.015$ ev. These values are in good agreement with the measurements of other experimenters.[54] As the spin of Au^{197} is $\frac{3}{2}$, the choices for the angular momentum of the compound nucleus are $J=1$ or 2, which give expected values for Γ_n/Γ of 0.15±0.01 or 0.093±0.005, respectively. Experimental values obtained for Γ_n/Γ are 0.14 by Harris *et al.*,[41] and 0.12±0.01 by Tittman and Sheer.[55] It thus appears that the accuracy of the measurements is not sufficient to make a definite assignment of J.

The parameters of the resonances up to 200 ev are summarized in Table VI. The calculated parameters are based on a value of Γ_γ of 0.15 ev. On the assumption that all the resonances below 200 ev have been resolved; the average level spacing for a single J in gold is 57 ev. The average value of Γ_n^0 for all the levels measured is 5 mv, with fluctuations of about the same magnitude as observed in iodine.

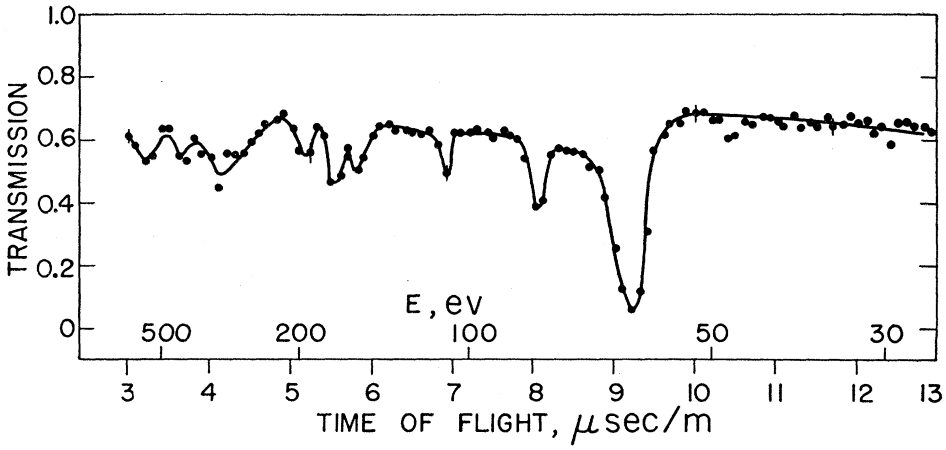

FIG. 24. The transmission as a function of neutron time of flight for a 12.3 g/cm² sample of Au^{197} metal. The only resonance below 30 ev is at 4.9 ev; above 200 ev individual levels were not resolved. The slope of the transmission curve between 30 and 50 ev and the asymmetry of the 61-ev level are caused by interference between resonance and potential scattering.

[54] H. H. Landon and V. L. Sailor, Phys. Rev. **93**, 1030 (1954).
[55] J. Tittman and C. Sheer, Phys. Rev. **83**, 746 (1951).

TABLE VI. A summary of the parameters of the levels from 0 to 200 ev in gold. Γ_γ is assumed to be 0.15 ev.

E_0 ev	Area ev	$(1/n)\times10^{24}$ cm²/atom	Δ ev	y	$\sigma_0\Gamma^2$ ev² b	$2g\Gamma_n$ mv	$2g\Gamma_n^0$ mv
4.94±0.04[a]					800±150	19 ± 2	8.5±0.9
61.5 ±1.0	6.5±1.0	33.5	0.18	1.00	450±130	90 ±30	11 ±3
80.2 ±1.5	2.1±0.4	33.5	0.20	1.09	41± 17		
	1.9±0.3	26.7		1.10	28± 9		
				Average	32± 8	12 ± 4	1.4±0.4
110 ±3	1.4±0.3	33.5	0.24	1.27	16± 8		
	1.2±0.3	26.7		1.33	9± 5		
				Average	12± 4	6.5± 3	0.6±0.3
153 ±4	2.7±0.7	33.5	0.28	1.10	70± 40	43 ±25	3.5±2
168 ±5	4.0±0.9	33.5	0.29	1.04	170± 80	90 ±40	7 ±3
194 ±6	2.5±0.7	33.5	0.32	1.17	55± 35	43 ±30	3 ±2
		$D=57$ ev			$\bar{\Gamma}_n^0=5$ mv		

[a] Parameters of this resonance are obtained by the "shape" analysis discussed in Sec. V D.

E. Thorium

Thorium was investigated because it is the heaviest monoisotopic element available and it was desired to make measurements over a large range of atomic weights. Transmission measurements of thorium metal were made in the energy region from 5 to 200 ev. Representative transmission curves, shown in Fig. 25 for sample thicknesses of 3.60, 11.0, and 22.1 g/cm², revealed several interesting features. The previously reported resonance[25] at about 20 ev was clearly resolved into two levels, separated by 1.7 ev. Furthermore, these two levels and the 71-ev level showed an asymmetry characteristic of the interference between resonance and potential scattering, which indicates that Γ_n is not negligible compared to Γ_γ. Thorium is a particularly favorable case in which to observe this interference phenomenon because it is monoisotopic and has zero spin; therefore the resonance scattering interferes with the entire potential scattering.

The parameters of the levels in thorium from zero to 140 ev are summarized in Table VII; above this energy

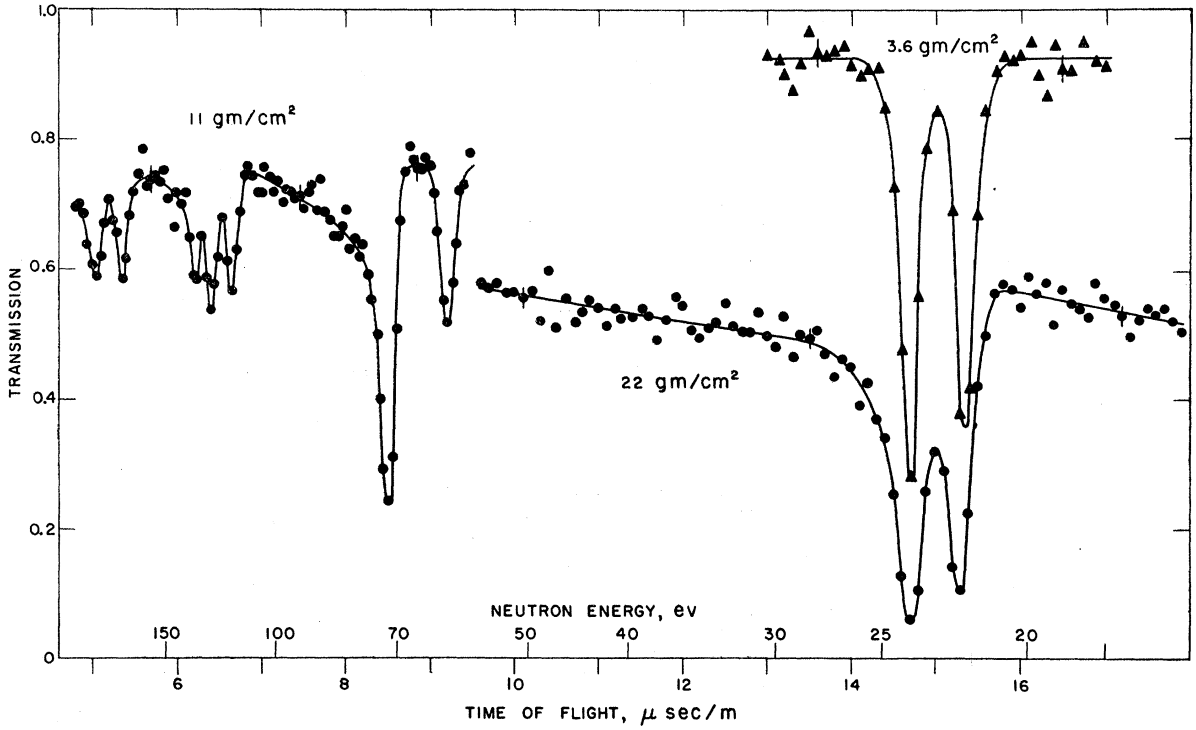

FIG. 25. The transmission as a function of neutron time of flight for samples of Th^{232} metal. There are no resonances below 20 ev; above 140 ev individual levels were not resolved. The two levels between 20 and 25 ev, which are well resolved with the thinnest sample, were not previously resolved by other experimenters. The asymmetry characteristic of interference between resonance and potential scattering is clearly seen in these two levels and the 71-ev level.

TABLE VII. A summary of the parameters of the levels from 0 to 140 ev in thorium. Γ_γ is assumed to be 30 mv.

E_0 ev	Area ev	$(1/n)\times10^{24}$ cm²/atom	Δ ev	y	$\sigma_0\Gamma^2$ ev² b	Γ_n[a] mv	Γ_n^0[a] mv
22.1±0.2	0.55±0.05	107	0.10	1.52	7± 2	1.8± 0.5	0.4±0.1
23.8±0.3	0.70±0.06	107	0.10	1.28	13± 4	3.5± 1.1	0.7±0.2
60.5±1.0	1.6 ±0.4	17.5	0.16	1.20	12± 5		
	1.1 ±0.2	35		1.60	8± 5		
				Average	10± 4	6.4± 2.5	0.8±0.3
70.8±1.3	1.9 ±0.3	107	0.17	1.04	120±40	44 ±20	5.2±2.5
117 ±3	1.2 ±0.2	35	0.23	2.04	7± 4	8 ± 5	0.8±0.5
127 ±3	1.6 ±0.3	35	0.24	1.33	20±10	20 ±10	1.7±0.9
133 ±3	1.3 ±0.3	35	0.24	1.88	10± 5	12 ± 6	1.1±0.6
		$D=20$ ev		$\bar{\Gamma}_n^0=1.5$ mv			

[a] Since $g=1$ for thorium, the last two columns give Γ_n and Γ_n^0, rather than $2g$ times these quantities.

the levels were not well resolved. The calculated parameters are based on a value of Γ_γ of only 30 mv,[43] which is much smaller, because of the large A, than the radiation widths of the other elements investigated in this paper. It should be noted that the fractional errors in the values of $\sigma_0\Gamma^2$ are larger than those for most of the other elements studied. The reason for this is twofold: first, the prominence of the interference between resonance and potential scattering requires the use of relatively thin samples in order that the measured area be due to the resonance cross section alone; second, Δ/Γ is very large for most of these levels (greater than 3 for all except the 71-ev level). These factors combine to give rather large values for the correction factor y, as well as large uncertainties in y due to the uncertainty in the measured area and in the assumed value of Γ_γ. The 64 ev² b value of $\sigma_0\Gamma^2$ measured by Hodgson *et al.*[25] for the 23-ev resonance in thorium is not correct because they failed to resolve the 22.1- and 23.8-ev levels. Their value could be nearly a factor of 2 larger than the sum of the value of $\sigma_0\Gamma^2$ for these two resonances, because their sample was thick and the calculated $\sigma_0\Gamma^2$ was proportional to the square of the measured area. If all the resonances below 140 ev have been resolved, the average level spacing in thorium is 20 ev and the average value of Γ_n^0 for these levels is 1.5 mv. Except for the large level at 71 ev, the values of Γ_n^0 are reasonably constant.

TABLE VIII. The values of level spacings (for single J values) at excitation energy equal to the neutron binding energy E^* determined from fast chopper data, and at E^*+1 Mev from fast neutron capture cross sections (see reference 1).

Target isotope	E^* Mev	$D(E^*)$, ev fast chopper	$D(E^*+1$ Mev), ev 1-Mev capture cross sections
Ag^{107}	7.4	50	6
Ag^{109}	7.0	33	2.7
I^{127}	7.3	29	3.3
Au^{197}	6.5	57	6[a]
Th^{232}	4.9	20	

[a] This value was computed from the capture cross section given in reference 1 by assuming $\Gamma_\gamma=0.15$ ev, rather than 0.03 ev assumed in that paper.

F. Discussion

The few isotopes whose level parameters have just been described represent only a beginning in the compilation of data needed for comparison with the results of nuclear structure theory. A definite attempt has been made in this work, however, to insure that all resonances of spin $I\pm\frac{1}{2}$ have been found in given energy regions. The results would be of little use if further improvement in resolution revealed still more levels in the same energy region. A number of isotopes not reported here have also been carefully studied with the fast chopper and the results presented briefly.[44–48]

One result that was soon evident is that the radiation widths show little variation. Although only a few measured values of Γ_γ are given here, the near-constancy is best shown in a recent survey of Hughes and Harvey,[43] which was based on fast chopper and other results. This behavior of the radiation widths is of interest theoretically, because of its connection with electric dipole transition probabilities, and practically, because it simplifies the analysis of resonances in the poor resolution region. The reduced neutron widths show a large variation relative to that of Γ_γ, but the measured widths are too few in number to draw any conclusions as yet on the distribution law of the Γ_n^0's. Enough cases are available, however, to reach significant conclusions, as we shall see, concerning the relationship of the average reduced neutron widths to the level spacings.

The directly observed average level spacings, D, correspond to the spacings of virtual levels of single J

TABLE IX. The observed average reduced neutron widths, average spacings (for single J values), and the ratio of these quantities.

Target isotope	No. of levels	$\bar{\Gamma}_n^0$ mv	D ev	$\bar{\Gamma}_n^0/D$ $\times10^4$
Ag^{107}	4	2.1	50	0.4
Ag^{109}	6	3.0	33	0.9
I^{127}	7	2.8	29	1.0
Au^{197}	7	5	57	0.9
Th^{232}	7	1.5	20	0.8

values ($I+\frac{1}{2}$ or $I-\frac{1}{2}$) at an excitation energy just above neutron binding energy. The observed cases are far too few to study variation of level spacing with even-odd effects, shell structure, etc. However, a rough comparison is possible with the level spacings inferred by Hughes, Garth, and Levin[1] from the capture cross sections for 1-Mev neutrons. These cross sections give the average level spacings at an excitation 1 Mev higher than neutron binding and contain some contributions from capture of neutrons with $l>0$. The radiation widths must also be assumed in the determination of the level density but this assumption now seems well justified.

In Table VIII are listed the level spacings obtained from the fast chopper results and from the 1-Mev cross sections. Both sets of D values for the isotopes studied seem to show little variation with atomic weight. The change in measured D with 1 Mev in energy is definite, about a factor of 10 for all the isotopes. It is difficult to estimate what part of this factor can be attributed to the contribution of higher l's in the 1-Mev results, and what part represents a decrease in level spacing for $l=0$. The results on level spacing are as yet too sketchy but they will be of definite value in relation to nuclear structure theory when many more are available.

It is instructive to consider the ratio of the average Γ_n^0 to D, which according to the strong-interaction theory of nuclear cross sections, should be independent of atomic weight and of neutron energy.[56] The value of this ratio, for a potential-well depth of 20 Mev, is predicted to be 1.4×10^{-4}. The observed ratios of the average reduced widths Γ_n^0 to the average spacing D are given in Table IX, from which it can be concluded that the observed ratio is indeed of the order of magnitude predicted and is reasonably constant. The average value for the ratio is 0.8×10^{-4}, which is slightly less than the value based on a 20-Mev well depth. However, it should be noted that the predicted value of 1.4×10^{-4} is based on the assumption of equidistant levels.[57] Any departure from this assumption would decrease the predicted value of the ratio; for example, for a random distribution of levels the predicted ratio is reduced by a factor of two.

[56] See reference 33, pp. 386–90.

ACKNOWLEDGMENTS

The authors wish to express their appreciation to the following people: Richard F. Randall, for his assistance in testing and maintaining the fast chopper and its associated equipment; the Electronics Division of Brookhaven National Laboratory, for work in the design, construction, and maintenance of the time-of-flight electronic analyzer; Charles P. Baker, for the use of his analyzer while the fast chopper analyzer was being constructed; Robert C. Garth and Herbert R. Muether, for their help in the early experimental work; Jane S. Levin, June C. Morris, and Marilyn S. Smith, for their assistance with the large amount of computation and plotting required in the analysis of the data and the preparation of curves; Edward Melkonian of Columbia University, for making the results of his calculations available to us before their publication. We also wish to thank John A. Harvey for his helpful criticism and valuable suggestions during the course of the experimental work and the preparation of this paper.

[57] Feshbach, Peaslee, and Weisskopf, Phys. Rev. **71**, 145 (1947).

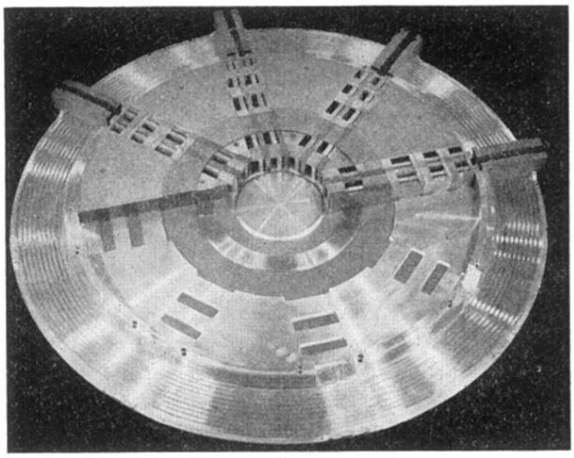

FIG. 3. A photograph of the partly assembled rotor. The 4 pairs of arms enclose the narrowest regions of 4 pairs of rotor slits. The rotor is made up of many pieces of plastic held between two aluminum forgings. It has a 30-in. diameter and weighs 250 pounds.

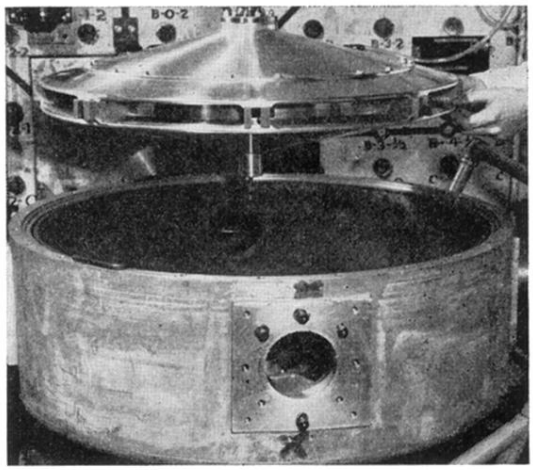

FIG. 4. A photograph of the assembled rotor and its housing. The rotor spins about a vertical axis. Entrance and exit stators are not in place. The pile shield is in the background.